



Bariatric surgery reveals a gut-restricted TGR5 agonist with anti-diabetic effects

Snehal N. Chaudhari^{1,3}, David A. Harris^{2,3}, Hassan Aliakbarian^{1,2}, James N. Luo^{1,2},
Matthew T. Henke¹, Renuka Subramaniam², Ashley H. Vernon², Ali Tavakkoli²,
Eric G. Sheu^{1,2}✉ and A. Sloan Devlin¹✉

Bariatric surgery, the most effective treatment for obesity and type 2 diabetes, is associated with increased levels of the incretin hormone glucagon-like peptide-1 (GLP-1) and changes in levels of circulating bile acids. The levels of individual bile acids in the gastrointestinal (GI) tract after surgery have, however, remained largely unstudied. Using ultra-high performance liquid chromatography–mass spectrometry-based quantification, we observed an increase in an endogenous bile acid, cholic acid-7-sulfate (CA7S), in the GI tract of both mice and humans after sleeve gastrectomy. We show that CA7S is a Takeda G-protein receptor 5 (TGR5) agonist that increases *Tgr5* expression and induces GLP-1 secretion. Furthermore, CA7S administration increases glucose tolerance in insulin-resistant mice in a TGR5-dependent manner. CA7S remains gut restricted, minimizing off-target effects previously observed for TGR5 agonists absorbed into the circulation. By studying changes in individual metabolites after surgery, the present study has revealed a naturally occurring TGR5 agonist that exerts systemic glucoregulatory effects while remaining confined to the gut.

Obesity and type 2 diabetes are medical pandemics. Bariatric surgery, in the form of roux-en-Y gastric bypass or sleeve gastrectomy (SG), is the most effective and lasting treatment for obesity and related comorbidities^{1,2}. For most patients, remission is durable and lasts for years post-surgery^{1,3}. Changes consistently observed after surgery include increased GLP-1, a circulating incretin hormone, and changes in the systemic bile acid (BA) repertoire⁴. BAs are cholesterol-derived metabolites that play crucial roles in host metabolism as detergents that aid in absorption of lipids and vitamins, and as ligands for host receptors⁵. BAs are implicated in post-SG therapeutic benefits due to their ability to mediate signaling through the G-protein-coupled receptor (GPCR) TGR5 (also known as GPBAR1)⁶ and the farnesoid X receptor (FXR, also known as NR1H4)⁶.

Thus far, research efforts have focused on overall changes in the total BA pool or in levels of conjugated or unconjugated BAs in circulating blood^{4,7}. Individual BAs, however, have different binding affinities for nuclear hormone receptors (NHRs) and GPCRs, and thus unique abilities to modulate glucose homeostasis, lipid accumulation and energy expenditure^{5,8}. It is not sufficient, therefore, to limit analyses to whole classes of BAs. Moreover, local activation of receptors in the intestine can affect global metabolic outcomes. In particular, GLP-1 is secreted postprandially by enteroendocrine L cells in the lower intestine in response to activation of TGR5, a GPCR with a primary role in energy metabolism⁹. GLP-1 stimulates pancreatic insulin release, and both hormones then regulate metabolism systemically¹⁰.

In the present study, we sought to identify specific naturally occurring BAs increased in the gut after SG and investigate the role of these compounds as TGR5 ligands and regulators of glucose metabolism. We identified one BA, CA7S (**1**), the levels of which were increased in cecal contents and feces of mice and

humans, respectively, after SG. We then determined that CA7S is a gut-restricted TGR5 agonist and GLP-1 secretagogue that improves systemic glucose clearance when administered to diet-induced obese mice in acute and chronic settings.

Results

CA7S is increased in mice and humans post-SG. SG is the most performed bariatric surgery in the USA owing to robust metabolic benefits and a favorable side-effect profile¹¹. Rodent SG models mimic the positive metabolic outcomes observed in humans and are suitable for studying post-surgical outcomes¹². In the present study, SG or sham surgery was performed on insulin-resistant, diet-induced obese (DIO) mice (Fig. 1a). SG mice displayed improved glucose tolerance and insulin sensitivity 4–5 weeks post-surgery compared with shams (Fig. 1b–e). SG mice also showed a reduction in percentage body weight compared with shams without differences in food intake between groups (see Supplementary Fig. 1a,b). Mice were euthanized 6 weeks post-surgery after an overnight fast and their tissues were harvested. Consistent with studies involving humans⁴, we observed an increase in circulating GLP-1 in SG mice (Fig. 1f).

BAs that are known agonists of TGR5 can induce GLP-1 secretion in lower-intestinal L cells^{4,9}. We therefore quantified individual BAs in cecal contents of SG and sham mice using ultra-high performance liquid chromatography–mass spectrometry (UPLC–MS) (Fig. 2a; for structures of all BAs in the text, figures, Extended Data and Supplementary Information, see Extended Data Fig. 1). We observed a significant increase in only one BA in cecal contents of SG mice ($P=0.03$). Based on its mass, this compound appeared to be a monosulfated metabolite of a trihydroxy-BA. We purified this compound from the pooled extracts of post-SG cecal contents using MS-guided semi-preparative HPLC. Using nuclear magnetic resonance (NMR) spectroscopy, we identified this compound as CA7S

¹Department of Biological Chemistry and Molecular Pharmacology, Harvard Medical School, Boston, MA, USA. ²Department of Surgery, Brigham and Women's Hospital, Harvard Medical School, Boston, MA, USA. ³These authors contributed equally: Snehal N. Chaudhari, David A. Harris.

✉e-mail: esheu@bwh.harvard.edu; sloan_devlin@hms.harvard.edu

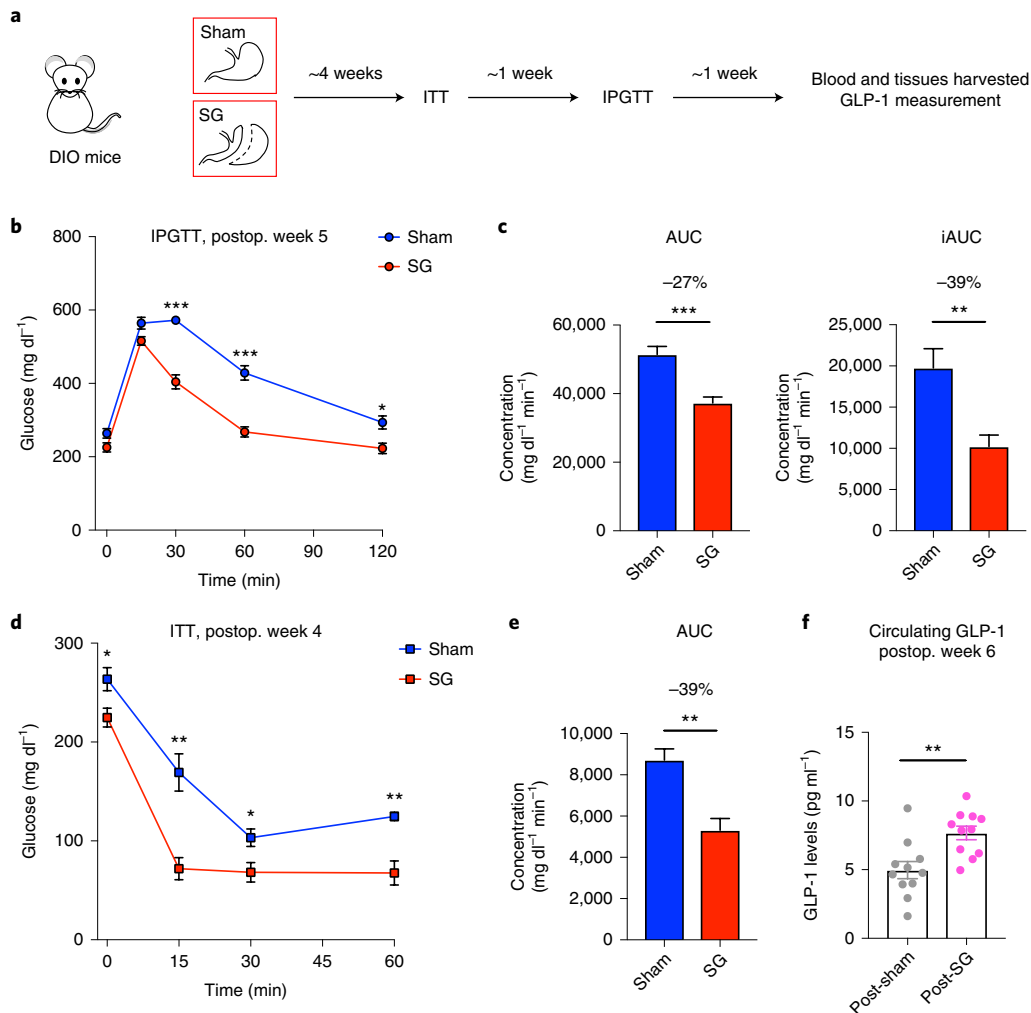


Fig. 1 | DIO mice display improved glucose tolerance and insulin sensitivity after SG. **a**, Schematic of surgical interventions and postoperative assessments. SG or sham surgery was performed on DIO mice, followed by an ITT -4 weeks postoperatively and then the IPGTT -5 weeks postoperatively. Blood and tissues were harvested -6 weeks postoperatively in the fasted state. **b**, Glycemic curves during IPGTT (SG, $n=7$; sham, $n=6$; 30 min: $***P=5.91 \times 10^{-6}$; 60 min: $***P=4.34 \times 10^{-5}$; 120 min: $*P=0.01$; two-tailed Student's *t*-tests). **c**, Corresponding blood glucose AUC and iAUC were reduced in SG- compared with sham-operated mice (SG, $n=7$; sham, $n=6$; AUC: $***P=4.01 \times 10^{-4}$; iAUC: $**P=6.12 \times 10^{-3}$; two-tailed Welch's *t*-tests). **d**, Glycemic curves during ITT (SG, $n=4$; sham, $n=4$; 0 min: $*P=0.04$; 15 min: $**P=4.31 \times 10^{-3}$; 30 min: $*P=0.03$; 60 min: $**P=4.53 \times 10^{-3}$; two-tailed Student's *t*-tests). **e**, Corresponding blood glucose AUC was reduced in SG- compared with sham-operated mice (SG, $n=4$; sham, $n=4$; AUC: $**P=5.25 \times 10^{-3}$, two-tailed Welch's *t*-test). **f**, GLP-1 levels were increased in mice post-SG compared with post-sham ($n=11$ per group, $**P=3.00 \times 10^{-3}$, two-tailed Welch's *t*-test). All data are presented as mean \pm s.e.m.

(Fig. 2b,c, and see also Supplementary Fig. 2 and Extended Data Fig. 2). CA7S is a sulfated metabolite of cholic acid (CA, 2), an abundant primary BA in both mice and humans. Sulfation of BAs predominantly occurs in the liver¹³. Consistent with this observation, we found increased levels of CA7S in the liver of SG mice (Fig. 2d). In agreement with previous studies, SG mice displayed increased levels of total circulating BAs (see Supplementary Fig. 3)⁷. However, there was no difference in total gut BA levels as measured in the cecal contents of post-SG and post-sham mice (Fig. 2c). Several BAs derived from the primary BA chenodeoxycholic acid (CDCA, 3) were decreased in mouse cecal contents, including lithocholic acid (LCA, 4), isolithocholic acid (isoLCA, 5) and CDCA. There was also a decrease in tauro-chenodeoxycholic acid (TCDCA, 6) and CDCA in mouse livers (see Extended Data Fig. 3 and Supplementary Fig. 4). Notably, CA7S was the only BA detected with levels that were significantly higher in SG mouse cecal contents and livers ($P=0.03$ and $P=0.03$, respectively).

To determine whether CA7S concentrations were also higher in humans after surgery, we quantified BAs in stool from patients who had undergone SG. We compared a preoperative with a postoperative stool sample collected from patients a median of 36 d after SG. Remarkably, even though total fecal BA levels were decreased in patients post-SG, fecal CA7S levels were significantly increased ($P=0.01$) (Fig. 2e). Consistent with our results from mouse cecal contents, we observed decreases in the CDCA-derived BAs isoLCA, LCA and ursodeoxycholic acid (UDCA, 7). CA, the putative substrate for production of CA7S, was also decreased in patients after surgery (see Extended Data Fig. 4). CA7S was the only BA detected with levels that were increased in patients post-SG (Fig. 2e). These data demonstrate that a specific BA metabolite, CA7S, is increased after SG in both mice and humans.

CA7S activates TGR5 and induces GLP-1 secretion in vitro. We next determined whether CA7S can activate TGR5 and induce

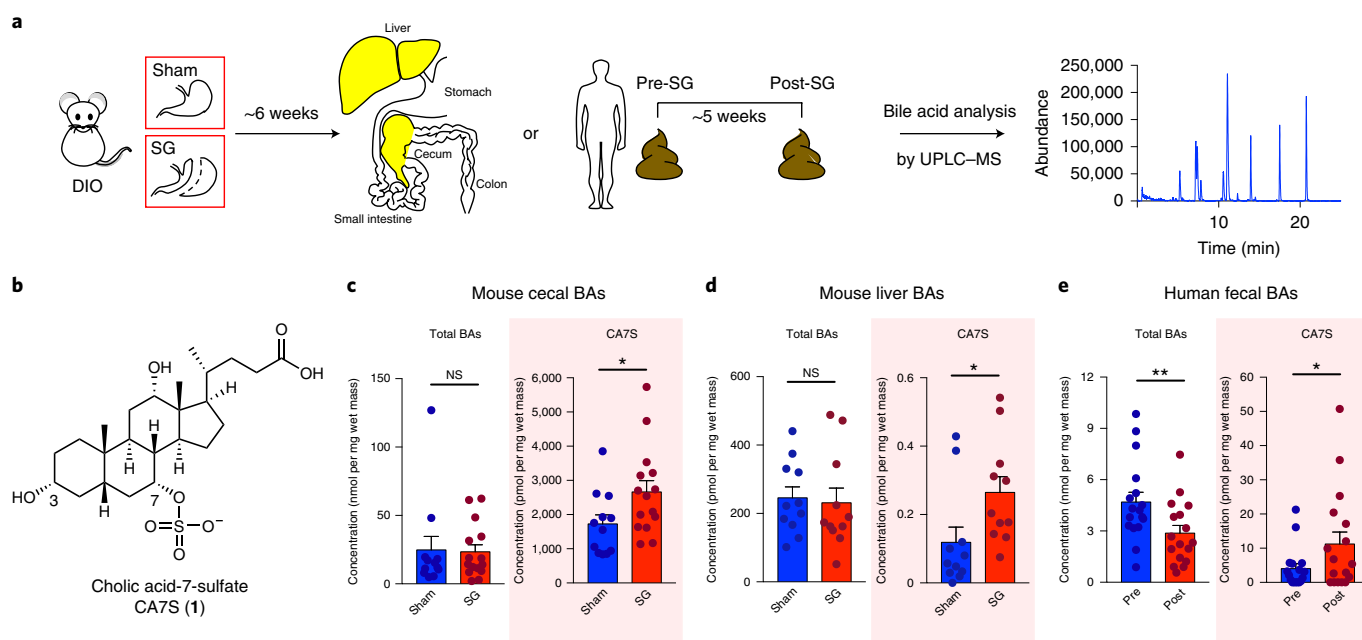


Fig. 2 | The BA metabolite CA7S is increased in mice and humans after SG. **a**, Schematic of sample collection followed by BA profiling using UPLC-MS. For mice, livers and cecal contents were collected from fasted sham or SG mice 6 weeks postoperatively. For humans, a preoperative stool sample was compared with a postoperative sample collected a median of 36 d after surgery. **b**, Structure of CA7S (**1**). **c**, CA7S was increased in the cecal contents of SG mice, whereas total BA concentrations did not differ between SG and sham mice (sham, $n=12$; SG, $n=15$; total BAs not significant (NS), $P=0.90$; CA7S, $*P=0.03$, two-tailed Welch's t -test). Note that 1 pmol BA per mg wet mass is approximately equivalent to 1 μM . **d**, CA7S was increased in the livers of SG mice (SG, $n=11$; sham, $n=11$, total BAs NS, $P=0.55$; CA7S, $*P=0.03$, two-tailed Welch's t -tests). **e**, CA7S in human feces was increased post-SG compared with pre-surgery ($n=17$ patients; total BAs, $**P=1.00 \times 10^{-3}$; CA7S, $*P=0.01$, two-tailed, paired Student's t -tests).

GLP-1 secretion from L cells. Previous work has shown that sulfation of natural BAs and synthetic analogs alters their TGR5 agonistic activity¹⁴. We therefore hypothesized that CA7S possessed altered TGR5 agonism compared with CA. Although sulfation at C3 abolishes TGR5 agonist activity of LCA (reported half-maximal effective concentration (EC_{50}) values of 0.03–3.70 μM and >100 μM for LCA and LCA-3-sulfate, respectively), replacement of the C24-carboxylic acid with a C24-sulfate lowers the EC_{50} of CA, CDCA and UDCA by an order of magnitude^{14–18}. We therefore hypothesized that the C7-sulfated version of CA, CA7S, might possess different TGR5 agonistic activities to CA, which is a weak agonist of TGR5 (reported EC_{50} of 7.72–27 μM)^{14–16,19,20}. We examined the activation of human TGR5 by CA7S, CA or taurodeoxycholic acid (TDCA, **8**) using a transient transfection assay in human embryonic kidney cells (HEK293T). TDCA is a naturally occurring BA and potent TGR5 agonist²¹. HEK293T cells were cotransfected with a cAMP response element (CRE)-driven luciferase reporter construct and human *Tgr5* expression plasmid. CA7S activated human TGR5 in a dose-dependent manner and to a similar extent to TDCA. CA7S also displayed a lower EC_{50} (0.17 μM) than CA (12.22 μM) (Fig. 3a). CA7S falls within the reported EC_{50} range of endogenous TGR5 ligands and is more potent than reported synthetic ligands (see Supplementary Table 1).

TDCA is currently one of the most potent, naturally occurring GLP-1 secretagogues known²¹. CA7S induced GLP-1 secretion in human intestinal L cells (NCI-H716) to a similar degree to TDCA in a dose-dependent manner. CA had no effect on GLP-1 secretion (Fig. 3b). CA7S extracted and purified directly from cecal contents of SG mice also induced GLP-1 secretion in vitro (see Extended Data Fig. 5a). Furthermore, short interfering (si)RNA-mediated knockdown of TGR5 abolished both CA7S- and TDCA-mediated secretion of GLP-1 (Fig. 3b and see also Extended Data Fig. 5b). This result indicates that induction of GLP-1 secretion by CA7S requires TGR5. TGR5 agonism also results in elevated intracellular

calcium levels²². We observed a dose-dependent increase in calcium levels in NCI-H716 cells treated with CA7S (see Extended Data Fig. 5c).

The BA repertoire in sham and SG mouse intestines as well as human feces includes molecules previously shown to be agonists of TGR5, including deoxycholic acid (DCA, **9**) (see Supplementary Table 1 and Extended Data Figs. 3 and 4)^{23,24}. To investigate whether CA7S can induce GLP-1 secretion in the presence of physiologically relevant amounts of DCA measured in human cecal contents²⁵, we incubated NCI-H716 cells with 200 μM DCA and varying concentrations of CA7S. As expected, adding DCA resulted in an increase in GLP-1 concentration compared with a dimethyl sulfoxide (DMSO) control (Fig. 3c). However, even when low concentrations of CA7S (0.1 μM) were added, GLP-1 secretion increased compared with DCA alone. Likewise, when NCI-H716 cells were incubated with a physiologically relevant concentration of LCA (150 μM), addition of 0.1 μM CA7S resulted in an increase in GLP-1 secretion (see Extended Data Fig. 5d). These results indicate that CA7S can increase GLP-1 secretion even in the presence of endogenous TGR5 agonists.

To further test whether CA7S can induce GLP-1 secretion in the complex BA milieu of the gut, we generated in vitro pools of BAs mimicking the average concentrations found in sham and SG mouse cecum, and tested their ability to induce GLP-1 secretion. The SG BA pool increased GLP-1 secretion compared with the sham pool (Fig. 3d). The SG pool generated without CA7S did not, however, induce GLP-1 secretion compared with either the sham pool or the DMSO control (Fig. 3d). Our results demonstrate that CA7S, a naturally occurring BA metabolite, is a potent TGR5 agonist that can activate this receptor in the presence of other endogenous TGR5 agonists to induce GLP-1 secretion.

CA7S induces TGR5 signaling and gene expression. We next examined the effects of CA7S on *Tgr5* expression. Some

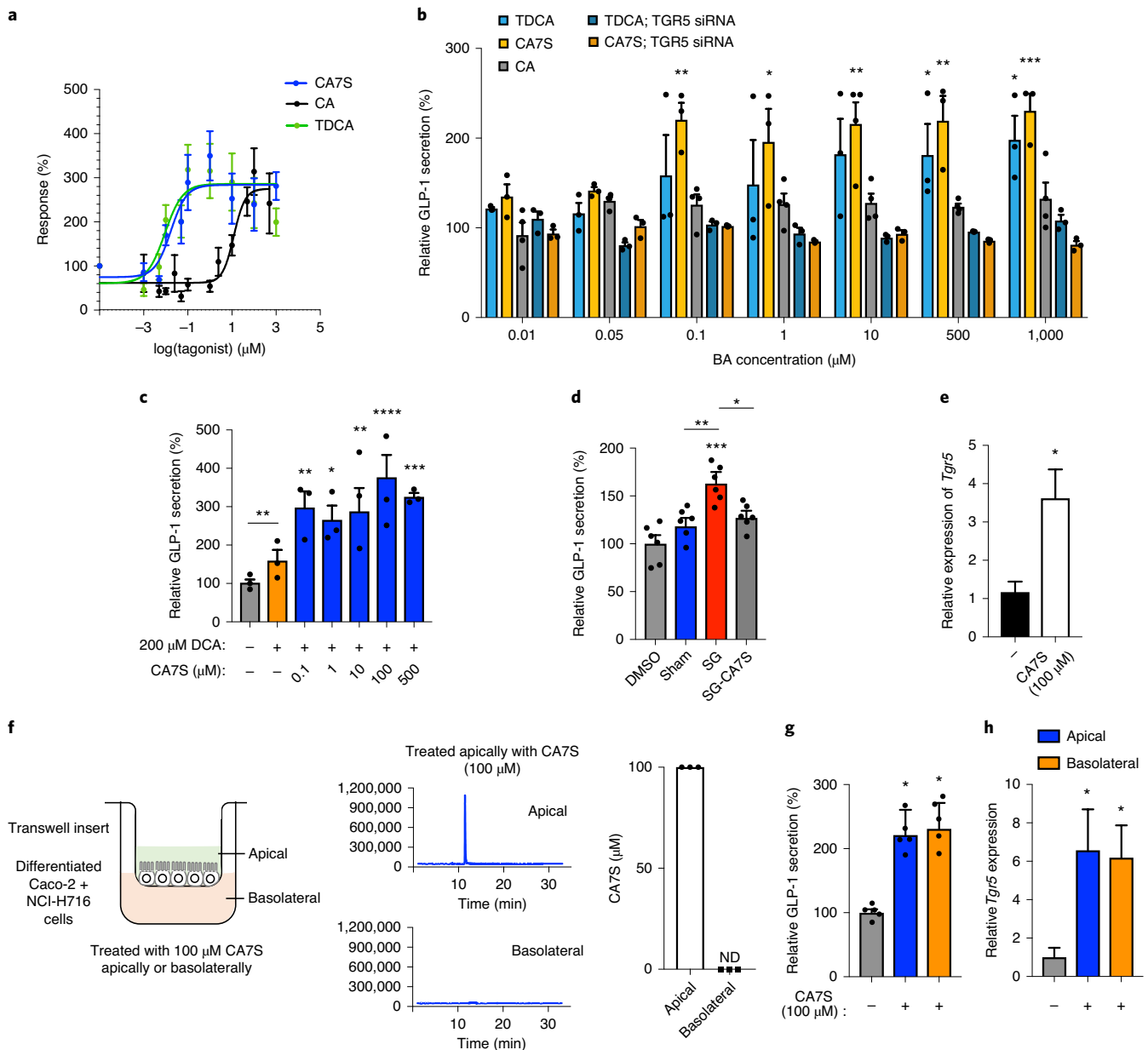


Fig. 3 | CA7S activates TGR5 signaling and increases *Tgr5* expression. **a**, Dose-response curves for human TGR5 activation in HEK293T cells overexpressing human *Tgr5* for CA7S, TDCA and CA (three biological replicates for CA and TDCA, six biological replicates for CA7S; see Supplementary Table 1 for EC₅₀ values). **b**, CA7S-induced secretion of GLP-1 in NCI-H716 cells compared with both CA and the known TGR5 agonist, TDCA. siRNA-mediated knockdown of *Tgr5* abolished GLP-1 secretion (three biological replicates for all except four biological replicates for CA; data not marked with asterisk(s) are not significant; CA7S: 0.1 μM $^{**}P=8.00 \times 10^{-3}$; 1 μM $^{*}P=0.03$; 10 μM $^{**}P=2.03 \times 10^{-3}$; 500 μM $^{**}P=3.00 \times 10^{-3}$; 1,000 μM $^{***}P=7.00 \times 10^{-4}$; TDCA: 500 μM $^{*}P=0.04$, 1,000 μM $^{*}P=0.02$; one-way ANOVA followed by Dunnett's multiple-comparison test). For reverse transcription (RT)-qPCR expression analysis of *Tgr5* knockdown, see Extended Data Fig. 5b,c. CA7S induced secretion of GLP-1 in the presence of a physiologically relevant concentration of DCA (200 μM) (three biological replicates per condition, DMSO (-) control versus DCA, not significant, $P=0.28$; 0.1 μM CA7S versus DCA $^{**}P=4.90 \times 10^{-3}$; 1 μM $^{*}P=0.03$; 10 μM $^{**}P=5.30 \times 10^{-3}$; 100 μM $^{****}P=1.00 \times 10^{-4}$; 500 μM $^{***}P=7.00 \times 10^{-4}$; two-way ANOVA followed by Dunnett's multiple-comparison test). **d**, In vitro pools of BAs mimicking the mean physiological concentrations of SG cecal BAs induced GLP-1 secretion in NCI-H716 cells compared with pools of mean sham cecal BAs. Induction of GLP-1 secretion by the SG cecal BA pool was lost when CA7S was removed from the pool (SG-CA7S) (six biological replicates per condition; data not marked with asterisk(s) are not significant; DMSO versus sham not significant, $P=0.52$; DMSO versus SG $^{***}P=7.00 \times 10^{-4}$; DMSO versus SG-CA7S not significant, $P=0.24$; sham versus SG $^{**}P=4.00 \times 10^{-3}$; SG versus SG-CA7S $^{*}P=0.03$; one-way ANOVA followed by Dunnett's multiple-comparison test). **e**, RT-qPCR analysis of *Tgr5* expression in NCI-H716 cells treated with CA7S (four biological replicates per condition, $^{*}P=0.01$, two-tailed Welch's *t*-test). **f**, Schematic of differentiated Caco-2 and NCI-H716 cells grown in transwells and treated with CA7S. Apical treatment of epithelial monolayer with 100 μM CA7S led to undetectable amounts of CA7S in the basolateral chamber as measured by UPLC-MS analysis (three biological replicates, representative UPLC-MS traces shown). ND, not detected. **g,h**, CA7S (100 μM) induced GLP-1 secretion (**g**) and *Tgr5* expression (**h**) when administered apically or basolaterally to a mixed monolayer of Caco-2 and NCI-H716 cells in a transwell system compared with control (five biological replicates per condition; apical CA7S $^{*}P=0.02$ and basolateral CA7S $^{*}P=0.01$ (**g**); apical CA7S $^{*}P=0.03$, basolateral CA7S $^{*}P=0.02$ (**h**); one-way ANOVA followed by Dunnett's multiple-comparison test). All data are presented as mean \pm s.e.m.

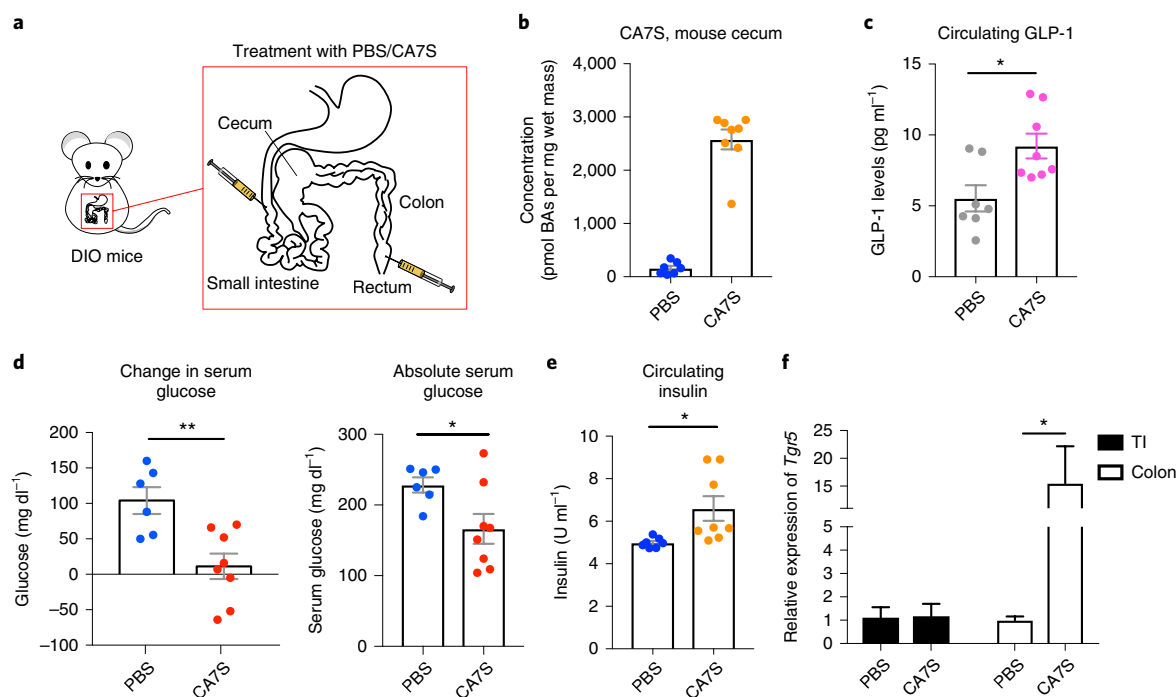


Fig. 4 | Acute CA7S administration induces GLP-1 and reduces serum glucose levels in vivo. **a**, Schematic of acute treatment wherein fasted DIO mice were anesthetized and treated with PBS or CA7S via duodenal and rectal catheters. **b**, Concentration of CA7S in the mouse cecum 15 min after treatment with PBS or CA7S (PBS, $n=7$; CA7S, $n=8$ mice). **c–e**, CA7S-treated mice displayed increased GLP-1 (**c**), reduced blood glucose levels (**d**) and increased blood insulin levels (**e**) compared with PBS-treated mice (PBS, $n=7$; CA7S, $n=8$ mice, $*P=0.01$ (**c**); $*P=0.02$ (**e**), two-tailed Welch's t -test; PBS, $n=6$; CA7S, $n=8$ mice, $**P=4.20 \times 10^{-3}$, $*P=0.02$, two-tailed Welch's t -tests (**d**)). **f**, CA7S treatment in the intestine induced *Tgr5* expression in the colon but not in the terminal ileum (TI) (PBS, $n=7$; CA7S, $n=8$ mice, $*P=0.03$, two-tailed Welch's t -test). All data are presented as mean \pm s.e.m.

small-molecule agonists of TGR5 can also increase *Tgr5* expression^{26–29}. To test whether CA7S induces *Tgr5* expression in addition to agonizing this receptor, we incubated NCI-H716 cells with 100 μ M CA7S and quantified *Tgr5* expression. We observed an increase in *Tgr5* expression within 2 h (Fig. 3e). BA derivatives that are FXR agonists or dual FXR/TGR5 agonists induce *Tgr5* expression via FXR activation^{26,27}. On the contrary, BAs and BA derivatives that are TGR5-specific agonists can induce *Tgr5* expression independent of FXR activation²⁶. CA7S did not activate endogenous FXR in human intestinal Caco-2 cells at all concentrations tested (see Extended Data Fig. 5e), suggesting that CA7S induces *Tgr5* expression through an FXR-independent mechanism.

Enteroendocrine L cells that secrete GLP-1 are distributed in the intestinal epithelial monolayer, particularly in the distal gut^{30,31}. *Tgr5* is expressed apically and basolaterally on these cells²¹. BA-mediated TGR5 agonism leading to GLP-1 secretion has been suggested to occur predominately with basolateral activation of TGR5 (ref. 21), a process that requires active or passive transport of BAs from the apical to the basolateral side of the intestinal epithelium²¹. However, sulfated BAs are poor substrates for intestinal BA transporters and are poorly absorbed^{13,26,27}, making apical activation a more likely route of TGR5 engagement by CA7S. To test whether CA7S can activate TGR5 apically, we differentiated a mixture of human intestinal epithelial Caco-2 cells and enteroendocrine NCI-H716 cells into polarized monolayers in a transwell system. These monolayers form a physical and biochemical barrier to the passage of small molecules, thus mimicking the gut epithelium^{32,33}. There was no detectable CA7S in the basolateral chamber after apical treatment with 100 μ M CA7S, suggesting that CA7S was neither actively nor passively transported to the basolateral side of the monolayer (Fig. 3f). Apical treatment of the monolayer with CA7S led to an increase in both GLP-1 secretion and *Tgr5* expression (Fig. 3g,h). Addition of CA7S (100 μ M) to the basolateral chamber also induced both GLP-1

secretion and *Tgr5* expression. However, as CA7S was not transported across the epithelium, basolateral administration of CA7S is likely not relevant to the in vivo mechanism of TGR5 activation. Thus, CA7S is a TGR5 agonist capable of inducing *Tgr5* expression and GLP-1 secretion from the apical side of intestinal epithelial cells.

Enteral CA7S induces GLP-1 and reduces blood glucose. We next evaluated the acute anti-diabetic effects of CA7S in vivo. After an overnight fast, DIO mice were administered either CA7S or phosphate-buffered saline (PBS) via duodenal and rectal catheters (Fig. 4a). Administration of 1 mg CA7S resulted in an average of 2,500 picomol per mg wet mass of CA7S in cecal contents, a concentration similar to observed post-SG levels (see Figs. 2c and 4b, and see also Supplementary Table 2). CA7S-treated mice displayed increased systemic GLP-1 levels compared with PBS-treated mice within 15 min (Fig. 4c). Moreover, CA7S-treated mice exhibited reduced blood glucose levels and increased insulin levels compared with PBS-treated mice (Fig. 4d,e and see also Extended Data Fig. 5f). Consistent with our in vitro results in L cells, *Tgr5* expression was increased in the colon of CA7S-treated mice (Fig. 4f). GLP-1-producing enteroendocrine L cells are known to be enriched in the colon compared with the small intestine^{30,31}. *Tgr5* expression was not increased in the terminal ileum of CA7S-treated mice (Fig. 4f). Analysis of individual BAs in the cecum, gallbladder and liver showed no differences in any other detectable BAs in CA7S-treated compared with PBS-treated mice (see Extended Data Fig. 6 and Supplementary Figs. 5 and 6). These results suggest that, in an acute setting, distal action of CA7S in the GI tract induces systemic glucose clearance and thus ameliorates hyperglycemia.

Oral CA7S administration increases glucose tolerance. To further study the anti-diabetic effects of CA7S, fasted DIO mice were orally gavaged with CA7S (100 mg kg⁻¹). Analysis of cecal contents

5 h post-gavage showed an average accumulation of 15,000 pmol per mg wet mass of CA7S (Fig. 5a), a concentration that is within an order of magnitude of the average in post-SG mice. Analysis of individual BAs in the cecum, gallbladder and liver showed no differences in any other BAs between the two groups (see Extended Data Fig. 7 and Supplementary Figs. 7 and 8). Systemic GLP-1 levels were increased in CA7S-gavaged mice compared with PBS-treated mice 5 h post-treatment (Fig. 5b). This result is consistent with the findings from enteral administration and demonstrates that oral CA7S treatment increases circulating GLP-1 for several hours.

We then determined the effect of CA7S on glucose tolerance over time using an oral glucose tolerance test (OGTT). DIO mice were gavaged with CA7S (100 mg kg⁻¹) or PBS and then administered an oral glucose bolus 3 h later. CA7S treatment resulted in an increased rate of blood glucose clearance (Fig. 5c). Moreover, the total and incremental areas under the glucose versus time curves (area under the curve (AUC) and incremental AUC (iAUC)) were decreased in CA7S-treated mice (Fig. 5d). These results demonstrate that CA7S increases blood glucose clearance after oral glucose challenge.

Anti-diabetic effects of CA7S require TGR5. CA7S is a potent inducer of GLP-1 secretion. We therefore sought to determine whether the acute anti-diabetic effects of CA7S depend on GLP-1. We performed lentiviral short hairpin (sh)RNA-mediated knockdown of the GLP-1 receptor (*Glp1r*) in vivo. DIO mice were injected intraperitoneally with 5 × 10⁵ shRNA lentiviral particles targeting *Glp1r*. At day 3 post-injection, *Glp1r* expression in the small intestine, heart and stomach was substantially reduced and, importantly, the *Glp1r* expression was undetectable in the pancreas (see Supplementary Fig. 9a). Mice were then gavaged with CA7S (100 mg kg⁻¹) or PBS and subjected to an OGTT 3 h later. For the final time point of the glycemic curve (120 min), CA7S-treated mice displayed lower blood glucose than PBS-treated mice. For all other time points and for the AUCs, there were no longer significant differences between the groups in the absence of GLP-1 receptor (GLP-1R), suggesting that, in an acute setting, the systemic glucose clearing effects of CA7S are partially dependent on the action of GLP-1 (Fig. 5e,f).

Previous studies have shown that SG confers anti-diabetic effects on mice lacking GLP-1R³⁴. However, the absence of TGR5 attenuates the anti-diabetic effects of SG³⁵. These results suggest that, although GLP-1R is not required for the anti-diabetic effects of SG, the presence of TGR5 is required. To determine whether the glucose-clearing effects of CA7S are dependent on TGR5, we performed lentiviral shRNA-mediated knockdown of *Tgr5* in vivo. Similar to the *Glp1r* knockdown, DIO mice were injected intraperitoneally with 5 × 10⁵ shRNA lentiviral particles targeting *Tgr5*. At day 3 post-injection, expression of *Tgr5* in the colon, the primary

site of action of CA7S, was markedly reduced (see Supplementary Fig. 9b). Mice were then gavaged with CA7S (100 mg kg⁻¹) or PBS and subjected to an OGTT 3 h later. In the absence of TGR5, the glycemic curves for CA7S- and PBS-treated animals were almost identical, with no differences in the AUC and iAUC metrics (Fig. 5g,h). Together, these data suggest that, in an acute setting, the systemic glucose-clearing effects of CA7S require TGR5 (Fig. 5g,h).

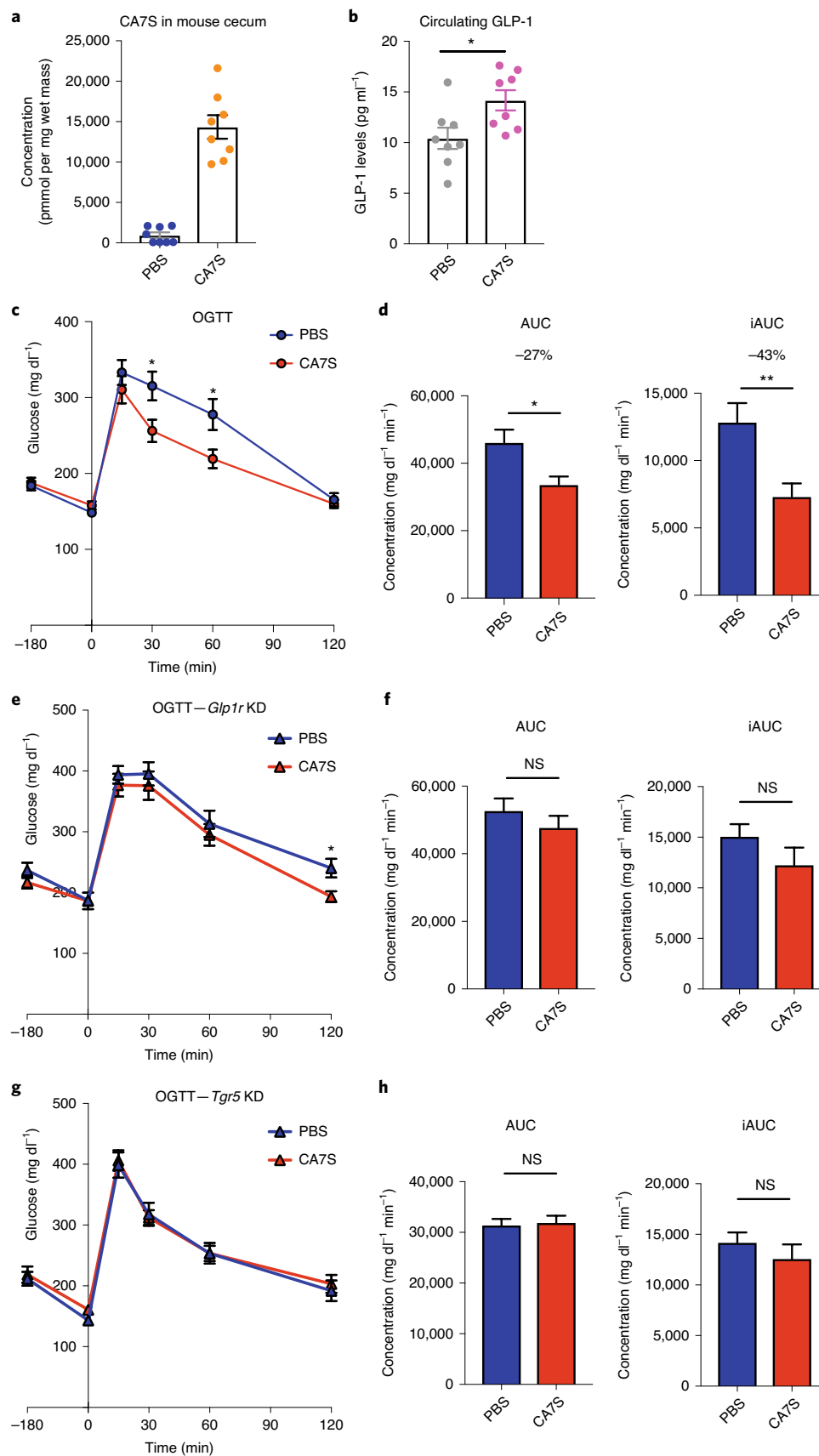
Long-term dosing with CA7S confers anti-diabetic effects. To assess the effects of chronic CA7S treatment, DIO mice were gavaged daily with 100 mg kg⁻¹ of CA7S or vehicle (PBS) for 48 d. Long-term oral gavage with CA7S or PBS led to an initial weight loss in all groups. There were no differences between groups in percentage body weight change at the end of the experiment or total food intake (see Supplementary Fig. 10a,b). On day 48, mice were euthanized after an overnight fast. CA7S gavage led to an accumulation of 30,000 pmol per mg wet mass of this compound in murine cecal contents (mean value; Fig. 6a). CA7S-dosed animals displayed higher circulating GLP-1 levels (Fig. 6b). Moreover, CA7S-treated mice exhibited reduced blood glucose levels and increased insulin levels compared with PBS-treated mice (Fig. 6c,d and see also Supplementary Fig. 10c). Thus, CA7S can improve diabetic phenotypes in DIO mice in a weight loss-independent manner. Chronic dosing with CA7S did not alter total levels of BAs in the cecum, gallbladder or liver (see Extended Data Fig. 8 and Supplementary Figs. 11 and 12). However, LCA and UDCA levels were decreased in cecal contents, similar to post-SG (see Extended Data Figs. 3, 4 and 8). Chronic CA7S treatment did not alter BA levels in the liver or gallbladder, suggesting that BA synthesis was unaffected (see Supplementary Figs. 11 and 12). Consistent with our enteral treatment results, mice dosed chronically with CA7S displayed increased colonic levels of *Tgr5* expression compared with the PBS-dosed mice (Fig. 6e). These results suggest that, in a chronic setting, CA7S induces GLP-1 secretion and ameliorates hyperglycemia.

CA7S is gut restricted and non-toxic. Although high concentrations of CA7S were observed in the intestine, this metabolite was undetectable in both circulating and portal venous blood from SG and sham-operated mice (see Supplementary Table 2), suggesting that CA7S is neither recycled via the enterohepatic circulation nor absorbed into the systemic circulation. In contrast, the known endogenous TGR5 agonists TDCA and DCA are found in the circulation in mice⁸. Introduction of CA7S via enteral administration or acute or chronic oral gavage resulted in only minor amounts in the circulation and portal venous blood (see Supplementary Table 2). These findings are consistent with previous observations that sulfated BAs, in particular 7 α -sulfated BAs, are poorly absorbed in the intestine¹³.

Fig. 5 | CA7S gavage induces GLP-1 and improves glucose tolerance in vivo via TGR5. **a**, Concentration of CA7S in mouse cecum 5 h after PBS or CA7S gavage. **b**, CA7S mice displayed increased GLP-1 levels 5 h post-gavage. Mice remained fasting for the time between gavage and blood collection for GLP-1 measurement ($n=8$ mice per group, $*P=0.02$, two-tailed Welch's t -test (**a,b**)). **c,d**, DIO mice treated with CA7S (100 mg kg⁻¹) displayed increased glucose tolerance compared with vehicle-treated mice 3 h post-gavage, as determined by an OGTT ($n=11$ mice per group). **c**, Glycemic curves during OGTT (data not marked with asterisk(s) are not significant; 30 min, $*P=0.02$; 60 min, $*P=0.02$; 120 min $P=0.6$; two-tailed Student's t -tests). **d**, Corresponding blood glucose AUC and iAUC were significantly reduced in CA7S-treated mice (AUC, $*P=0.01$; iAUC, $**P=4.00 \times 10^{-3}$; two-tailed Welch's t -tests). **e,f**, On day 3 after treatment with lentiviral shRNA targeting GLP-1 receptor (*Glp1r*), CA7S (100 mg kg⁻¹) or PBS was administered and 3 h later, an OGTT was performed ($n=11$ mice per group). **e**, Glycemic curves during OGTT (data not marked with asterisk(s) are not significant; 30 min, $P=0.53$; 60 min, $P=0.53$; 120 min, $*P=0.02$; two-tailed Student's t -tests). KD, knockdown. **f**, Corresponding blood glucose AUC and iAUC were not significantly different in CA7S- or PBS-treated mice in which the *Glp1r* had been knocked down (AUC, $P=0.35$; iAUC, $P=0.20$; two-tailed Welch's t -tests). **g,h**, On day 3 after treatment with lentiviral shRNA targeting *Tgr5*, CA7S (100 mg kg⁻¹) or PBS was administered and, 3 h later, an OGTT was performed ($n=9$ mice per group). **g**, Glycemic curves during OGTT (data not marked with asterisk(s) are not significant; 30 min, $P=0.87$; 60 min, $P=0.85$; 120 min, $P=0.52$; two-tailed Student's t -tests). **h**, Corresponding blood glucose AUC and iAUC were not significantly different in CA7S- or PBS-treated mice in which the *Tgr5* had been knocked down (AUC, $P=0.56$; iAUC, $P=0.97$; two-tailed Welch's t -tests). For RT-qPCR expression analysis of *Glp1r* and *Tgr5* knockdown in **e,f** and **g,h**, respectively, see Supplementary Fig. 9.

Although synthetic TGR5 agonists ameliorate diabetic phenotypes³⁶, their therapeutic use is hampered by side effects resulting from their absorption into the circulation^{36,37}. Systemically absorbed

TGR5 agonists reduce bile secretion and induce gallbladder filling, thereby causing bile stasis^{9,37}. We did not observe any change in gallbladder weight in DIO mice 5 h post-CA7S gavage compared with



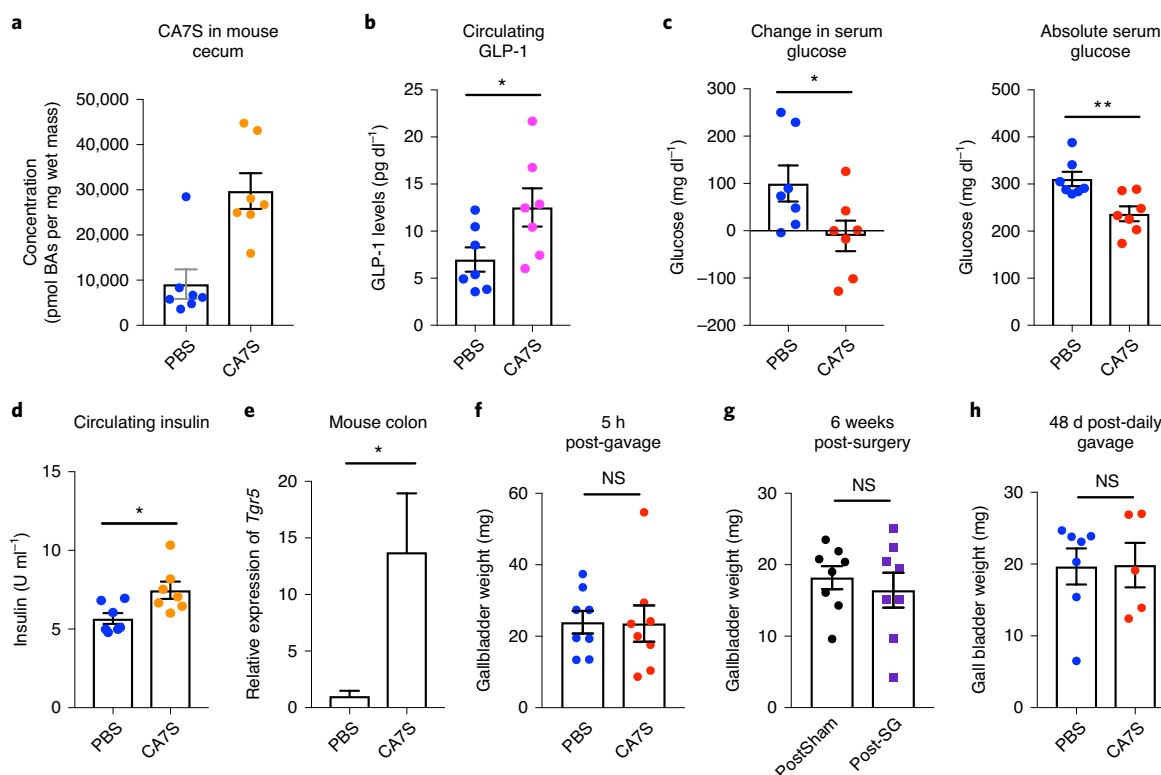


Fig. 6 | CA7S displays anti-diabetic effects in a chronic setting and does not affect gallbladder filling. **a**, Concentration of CA7S in mouse cecum at day 48 ($n=7$ in each group, animals were fasted overnight before euthanasia). **b–e**, CA7S-dosed mice displayed increased GLP-1 (**b**), reduced blood glucose levels (**c**), increased blood insulin levels (**d**) and increased *Tgr5* expression in the colon (**e**) compared with PBS-dosed mice ($n=7$ mice in each group (**b–e**); two-tailed Welch's *t*-tests). **f–h**, Administration of CA7S did not induce gallbladder filling in mice. **f**, Gallbladder weights were measured 5 h post-gavage with CA7S or PBS ($n=8$ mice per group, $P=0.95$, two-tailed Welch's *t*-test). **g**, Gallbladder weights were measured 6 weeks post-sham or post-SG surgery ($n=8$ mice per group; $P=0.56$; two-tailed Welch's *t*-test). **h**, Gallbladder weights were measured after 48 d of once-daily gavage with CA7S or PBS (PBS $n=7$, CA7S $n=5$ mice; $P=0.96$; two-tailed Welch's *t*-test). All data are presented as mean \pm s.e.m.

PBS treatment (Fig. 6f). In addition, SG did not induce a change in gallbladder weight despite increased CA7S levels (Fig. 6g). There was also no difference in individual BAs or total BA levels in sham versus SG gallbladders (see Supplementary Fig. 13). Furthermore, chronic CA7S treatment did not affect gallbladder weight (Fig. 6h). These results suggest that, in both acute and chronic settings, CA7S does not display one of the major side effects of non-gut-restricted TGR5 agonists.

High intestinal BA concentrations can damage the gut epithelium, an effect that can lead to inflammation and disruption of intestinal homeostasis³⁸. To determine whether CA7S disrupts gut epithelial barrier integrity, we tested the effect of CA7S on permeability using differentiated Caco-2 cell monolayers in a transwell system (see Supplementary Fig. 14). Epithelial permeability was assayed by measuring permeability to FITC dextran (FITC-D) after apical treatment with 1 mM CA7S for 12 h. Negligible amounts of CA7S were detected in the basolateral chamber, and there was no increase in FITC-D permeability, suggesting that CA7S remains gut restricted and does not affect the intestinal epithelial integrity (see Supplementary Fig. 14a,b). Furthermore, CA7S did not affect the viability of Caco-2 cells up to 15 mM (see Supplementary Fig. 14c), indicating that this metabolite is not toxic to human intestinal cells at physiologically relevant concentrations. In addition, CA7S is stable at physiological pH values (see Supplementary Fig. 14d). Together, these results suggest that oral administration of CA7S leads to delivery to the lower intestine without absorption or damage to the intestinal epithelium.

BA analysis after acute and chronic CA7S treatment showed that CA7S administration did not affect the total BA pool, nor did this treatment increase other BAs in the cecum (see Extended Data Figs. 6–8 and Supplementary Figs. 5–8, 11 and 12). To determine whether CA7S interacts with other host receptors, we screened CA7S against a panel of 19 NHRs and 169 GPCRs for agonist and antagonist activities. CA7S did not appreciably agonize or antagonize any receptor tested (see Supplementary note). Therefore, CA7S appears to exert anti-diabetic effects without affecting overall BA synthesis or BA signaling pathways.

Discussion

By quantifying changes in individual BAs, we found that the sulfated metabolite CA7S is increased in both the mouse GI tract and human feces after SG. We then found that CA7S is a potent TGR5 agonist that induces the secretion of the incretin hormone, GLP-1, from enteroendocrine L cells both in vitro and in vivo. In acute and chronic settings, we observed that CA7S exhibits anti-diabetic effects, including decreasing blood glucose levels and increasing glucose tolerance in insulin-resistant mice. Unlike known endogenous TGR5 agonists, CA7S is not absorbed into the portal or systemic circulation. Moreover, CA7S increased gene expression of its target receptor TGR5 in vitro and in vivo. Our knockdown experiments demonstrated that, in an acute setting, TGR5 is necessary for the in vivo efficacy of CA7S.

The finding that CA7S is a novel TGR5 agonist that improves glucose tolerance is noteworthy. CA7S had previously been regarded

as a metabolic waste product produced by the liver—a sulfated form of cholic acid that was tagged for excretion in the feces¹³. To our knowledge, no role for CA7S as a ligand for a GPCR or NhR has been reported. Our data indicate that CA7S is a signaling molecule that binds to TGR5 exclusively in the gut and increases systemic levels of GLP-1.

CA7S both agonizes and increases the gene expression of TGR5. This dual activity raises the possibility that CA7S may function in vivo through both direct and indirect mechanisms. Therefore, a portion of the anti-diabetic effects of CA7S may occur by upregulation of TGR5 with subsequent TGR5 agonism, not only by CA7S, but also by other abundant endogenous ligands, including DCA and LCA. Alternative mechanisms of action by CA7S in the presence of high concentrations of other ligands cannot be ruled out. In addition, the mechanism by which CA7S increases *Tgr5* expression is currently unknown, because this compound did not agonize FXR in our studies. These questions warrant further study.

Owing to the significant off-target effects caused by TGR5 agonists absorbed into the circulation, a gut-restricted TGR5 agonist has been suggested as a potential improved therapeutic for type 2 diabetes³⁷. Our data indicate that CA7S is a gut-restricted TGR5 agonist. CA7S was neither actively nor passively transported across a gut epithelial monolayer, did not disrupt epithelial barrier integrity and could activate TGR5 apically in vitro. In addition, acute and chronic in vivo administrations led to low to undetectable levels of CA7S in the portal and systemic circulations. CA7S does not induce gallbladder filling as has been reported for synthetic TGR5 agonists that enter the circulation. Furthermore, CA7S is not toxic to human intestinal cells and is stable at physiological pH values. Additional studies are required to assess the long-term effects of CA7S on weight loss and food intake. Nevertheless, as a result of its beneficial acute metabolic effects, gut restriction and low toxicity, CA7S could be a candidate for the development of a type 2 diabetes therapeutic.

The role that CA7S plays in the metabolic changes observed post-SG remains unknown. Due to the redundancy of sulfotransferases, the enzymes responsible for hepatic CA7S synthesis³⁹, knockdown of endogenous CA7S levels may be challenging. If this obstacle could be overcome, performing SG on CA7S-depleted mice would help reveal the contribution of this molecule to the metabolic effects of the surgery. We observed decreases in other BAs post-SG. Levels of CDCA were decreased in mouse cecal contents and liver, levels of UDCA were decreased in human feces post-SG, and levels of LCA and isoLCA were decreased in both mouse cecal contents and human feces. CDCA is an FXR agonist and LCA is a TGR5 agonist, whereas UDCA is relatively inert toward FXR and TGR5 (ref. ⁴⁰). FXR and TGR5 agonism has been shown to induce metabolic benefits, including increased glucose tolerance^{6,35,41}. Thus, decreases in levels of these metabolites post-SG would seem to oppose the anti-hyperglycemic effects of the surgery. It is interesting that we observed similar decreases in CDCA, LCA and UDCA levels in cecal contents of mice chronically treated with CA7S. Further research may reveal whether and how these compounds contribute to metabolic effects post-SG.

Our knockdown studies suggest that the anti-diabetic effects of CA7S are partially dependent on GLP-1R and dependent on TGR5. Our work is consistent with previous studies that have found that the absence of TGR5 and not GLP-1R attenuates post-SG anti-diabetic effects^{34,35}. These results raise the possibility that GLP-1-independent processes downstream of TGR5 may contribute to the increase in glucose tolerance caused by CA7S. TGR5 is broadly expressed in a variety of cell types, including immune, fat and liver cells⁴². Future work may elucidate other TGR5-dependent mechanisms through which CA7S exerts its glucose-lowering effects. More broadly, previously there were no known individual metabolites with levels that were altered by bariatric surgery and could increase blood glucose clearance. Through the identification and study of CA7S, we have

uncovered a metabolite that, although restricted to the GI tract, can improve global glucose regulation.

Online content

Any Nature Research reporting summaries, extended data, supplementary information, acknowledgements, peer review information; details of author contributions and competing interests; and statements of data and code availability are available at <https://doi.org/10.1038/s41589-020-0604-z>.

Received: 3 October 2019; Accepted: 1 July 2020;

Published online: 03 August 2020

References

1. Batterham, R. L. & Cummings, D. E. Mechanisms of diabetes improvement following bariatric/metabolic surgery. *Diabetes Care* **39**, 893–901 (2016).
2. Gloy, V. L. et al. Bariatric surgery versus non-surgical treatment for obesity: a systematic review and meta-analysis of randomised controlled trials. *BMJ* **347**, f5934–f5934 (2013).
3. Abbasi, J. Unveiling the ‘magic’ of diabetes remission after weight-loss surgery. *JAMA* **317**, 571–574 (2017).
4. Kaska, L., Sledzinski, T., Chomiczewska, A., Dettlaff-Pokora, A. & Swierczynski, J. Improved glucose metabolism following bariatric surgery is associated with increased circulating bile acid concentrations and remodeling of the gut microbiome. *World J. Gastroenterol.* **22**, 8698–8719 (2016).
5. Fiorucci, S. & Distrutti, E. Bile acid-activated receptors, intestinal microbiota, and the treatment of metabolic disorders. *Trends Mol. Med.* **21**, 702–714 (2015).
6. Ryan, K. K. et al. FXR is a molecular target for the effects of vertical sleeve gastrectomy. *Nature* **509**, 183–188 (2014).
7. Patti, M.-E. et al. Serum bile acids are higher in humans with prior gastric bypass: potential contribution to improved glucose and lipid metabolism. *Obesity* **17**, 1671–1677 (2009).
8. Sayin, S. I. et al. Gut microbiota regulates bile acid metabolism by reducing the levels of tauro-beta-muricholic acid, a naturally occurring FXR antagonist. *Cell Metab.* **17**, 225–235 (2013).
9. Duboc, H., Taché, Y. & Hofmann, A. F. The bile acid TGR5 membrane receptor: from basic research to clinical application. *Dig. Liver Dis.* **46**, 302–312 (2014).
10. Madsbad, S. The role of glucagon-like peptide-1 impairment in obesity and potential therapeutic implications. *Diabetes Obes. Metab.* **16**, 9–21 (2014).
11. Khorgami, Z. et al. Trends in utilization of bariatric surgery, 2010–2014: sleeve gastrectomy dominates. *Surg. Obes. Relat. Dis.* **13**, 774–778 (2017).
12. Lutz, T. A. & Bueter, M. The use of rat and mouse models in bariatric surgery experiments. *Front. Nutr.* **3**, 25 (2016).
13. Alnouti, Y. Bile acid sulfation: a pathway of bile acid elimination and detoxification. *Toxicol. Sci.* **108**, 225–246 (2009).
14. Sato, H. et al. Novel potent and selective bile acid derivatives as TGR5 agonists: biological screening, structure–activity relationships, and molecular modeling studies. *J. Med. Chem.* **51**, 1831–1841 (2008).
15. Kawamata, Y. et al. A G protein-coupled receptor responsive to bile acids. *J. Biol. Chem.* **278**, 9435–9440 (2003).
16. Maruyama, T. et al. Identification of membrane-type receptor for bile acids (M-BAR). *Biochem. Biophys. Res. Commun.* **298**, 714–719 (2002).
17. Sato, H. et al. Anti-hyperglycemic activity of a TGR5 agonist isolated from *Olea europaea*. *Biochem. Biophys. Res. Commun.* **362**, 793–798 (2007).
18. Rizzo, G. et al. Functional characterization of the semisynthetic bile acid derivative INT-767, a dual farnesoid X receptor and TGR5 agonist. *Mol. Pharmacol.* **78**, 617–630 (2010).
19. Pellicciari, R. et al. Discovery of 6alpha-ethyl-23(S)-methylcholic acid (S-EMCA, INT-777) as a potent and selective agonist for the TGR5 receptor, a novel target for diabetes. *J. Med. Chem.* **52**, 7958–7961 (2009).
20. Thomas, C. et al. TGR5-mediated bile acid sensing controls glucose homeostasis. *Cell Metab.* **10**, 167–177 (2009).
21. Brighton, C. A. et al. Bile acids trigger GLP-1 release predominantly by accessing basolaterally located G protein-coupled bile acid receptors. *Endocrinology* **156**, 3961–3970 (2015).
22. Kuhre, R. E. et al. Peptide production and secretion in GLUTag, NCI-H716, and STC-1 cells: a comparison to native L-cells. *J. Mol. Endocrinol.* **56**, 201–211 (2016).
23. Kuhre, R. E. et al. Bile acids are important direct and indirect regulators of the secretion of appetite- and metabolism-regulating hormones from the gut and pancreas. *Mol. Metab.* **11**, 84–95 (2018).
24. Guo, C., Chen, W.-D. & Wang, Y.-D. TGR5, not only a metabolic regulator. *Front Physiol.* **7**, 646 (2016).
25. Hamilton, J. P. et al. Human cecal bile acids: concentration and spectrum. *Am. J. Physiol. Gastrointest. Liver Physiol.* **293**, G256–G263 (2007).

26. Comeglio, P. et al. INT-767 prevents NASH and promotes visceral fat brown adipogenesis and mitochondrial function. *J. Endocrinol.* **238**, 107–127 (2018).
 27. Pathak, P. et al. Farnesoid X receptor induces Takeda G-protein receptor 5 cross-talk to regulate bile acid synthesis and hepatic metabolism. *J. Biol. Chem.* **292**, 11055–11069 (2017).
 28. Chen, M.-C., Chen, Y.-L., Wang, T.-W., Hsu, H.-P. & Lai, M.-D. Membrane bile acid receptor TGR5 predicts good prognosis in ampullary adenocarcinoma patients with hyperbilirubinemia. *Oncol. Rep.* **36**, 1997–2008 (2016).
 29. Xiong, Q. et al. Metabolite-sensing G protein coupled receptor TGR5 protects host from viral infection through amplifying type I interferon responses. *Front Immunol.* **9**, 2289 (2018).
 30. Eissele, R. et al. Glucagon-like peptide-1 cells in the gastrointestinal tract and pancreas of rat, pig and man. *Eur. J. Clin. Invest.* **22**, 283–291 (1992).
 31. Harach, T. et al. TGR5 potentiates GLP-1 secretion in response to anionic exchange resins. *Sci. Rep.* **2**, 430 (2012).
 32. Ferruzza, S., Rossi, C., Scarino, M. L. & Sambuy, Y. A protocol for differentiation of human intestinal Caco-2 cells in asymmetric serum-containing medium. *Toxicol. Vitro.* **26**, 1252–1255 (2012).
 33. Tan, H.-Y. et al. A multi-chamber microfluidic intestinal barrier model using Caco-2 cells for drug transport studies. *PLoS ONE* **13**, e0197101 (2018).
 34. Wilson-Pérez, H. E. et al. Vertical sleeve gastrectomy is effective in two genetic mouse models of glucagon-like peptide 1 receptor deficiency. *Diabetes* **62**, 2380–2385 (2013).
 35. McGavigan, A. K. et al. TGR5 contributes to glucoregulatory improvements after vertical sleeve gastrectomy in mice. *Gut* **66**, 226–234 (2017).
 36. Hodge, R. J. & Nunez, D. J. Therapeutic potential of Takeda-G-protein-receptor-5 (TGR5) agonists. Hope or hype? *Diabetes Obes. Metab.* **18**, 439–443 (2016).
 37. Cao, H. et al. Intestinally-targeted TGR5 agonists equipped with quaternary ammonium have an improved hypoglycemic effect and reduced gallbladder filling effect. *Sci. Rep.* **6**, 28676 (2016).
 38. Wang, S. et al. Interplay between bile acids and the gut microbiota promotes intestinal carcinogenesis. *Mol. Carcinog.* **58**, 1155–1167 (2019).
 39. Dawson, P. A. & Setchell, K. D. R. Will the real bile acid sulfotransferase please stand up? Identification of Sult2a8 as a major hepatic bile acid sulfonating enzyme in mice. *J. Lipid Res.* **58**, 1033–1035 (2017).
 40. Beuers, U., Trauner, M., Jansen, P. & Poupon, R. New paradigms in the treatment of hepatic cholestasis: from UDCA to FXR, PXR and beyond. *J. Hepatol.* **62**, S25–S37 (2015).
 41. Ma, K., Saha, P. K., Chan, L. & Moore, D. D. Farnesoid X receptor is essential for normal glucose homeostasis. *J. Clin. Invest.* **116**, 1102–1109 (2006).
 42. Schaap, F. G., Trauner, M. & Jansen, P. L. M. Bile acid receptors as targets for drug development. *Nat. Rev. Gastroenterol. Hepatol.* **11**, 55–67 (2014).
- Publisher's note** Springer Nature remains neutral with regard to jurisdictional claims in published maps and institutional affiliations.
- © The Author(s), under exclusive licence to Springer Nature America, Inc. 2020

Methods

Animals. DIO male C57Bl/6j mice aged 11, 13 and 16 weeks were purchased from the Jackson Laboratory for sham and SG surgeries, enteral CA7S treatment and all other nonsurgical experiments, respectively. Mice are placed on a high-fat diet (HFD) starting at age 6 weeks at the Jackson Laboratory. On receipt, animals were housed in a climate-controlled environment with 12 h light:dark cycles and continued on an HFD (60% kcal fat; Research Diets, catalog no. RD12492). Animals were acclimated for at least 1 week before undergoing procedures. Euthanasia was performed in the fasted state to minimize the confounding effects of varying food intake between mice and to allow for accurate fasting glucose and GLP-1 measurements. Animals were cared for according to the American Association for Laboratory Animal Science guidelines.

SG and sham procedures. The 11-week-old DIO mice were weight matched and either underwent SG or a sham operation after a 1-week acclimation. SG was performed through a 1.5-cm laparotomy under isoflurane anesthesia. The stomach was dissected free from its attachments, the vessels between the spleen and stomach (short gastric vessels) ligated, and a tubular stomach was created by removing 80% of the glandular and 100% of the nonglandular stomach with a linear-cutting surgical stapler. The sham operation consisted of laparotomy, stomach dissection, ligation of short gastric vessels and manipulation of the stomach along the staple line equivalent. Mice were individually housed thereafter to allow for monitoring of food intake, weight and behavior. Mice were maintained on Recovery Gel Diet (Clear H₂O) from 1 d before to 6 d after surgery, and an HFD was restarted on the morning of postoperative day (POD) 7. Mice were euthanized 5–7 weeks post-surgery after an overnight fast (17:00 to 07:00).

Functional glucose testing. After a 4-h fast (08:00 to 12:00), intraperitoneal glucose tolerance testing (IPGTT) and insulin tolerance testing (ITT) were performed at postoperative weeks 4 and 5, respectively. During IPGTT, mice received 2 mg g⁻¹ of intraperitoneal D-glucose (Sigma-Aldrich). Serum glucose levels were measured from the tail vein at 15, 30, 60 and 120 min with a OneTouch Glucometer (Life Technologies). ITT was performed by intraperitoneal instillation of 0.6 μg kg⁻¹ of regular human insulin (Eli Lilly and Company). Serum glucose was measured at 15, 30 and 60 min. Baseline glucose was measured before medication administration.

Body weight and food intake measurements. Sham and SG-operated mice were individually housed and weighed daily for the first postoperative week and then twice weekly until euthanasia. Food intake was measured twice weekly and daily food intake was calculated by averaging the grams eaten per day over the preceding days. For sham and SG-operated animals, food intake measurements were started on POD 10 because animals were transitioned from gel to HFD on POD 7. For chronic CA7S experiments, mice were weighed and food intake was measured daily until euthanasia.

BA analysis. BA analyses were performed using a previously reported method⁴³.

Reagents. Stock BA solutions were prepared in molecular biology-grade DMSO (VWR International) and were used to establish standard curves. CA7S was purchased from Cayman Chemicals (catalog no. 9002532). Glycocholic acid (GCA) (Sigma) was used as the internal standard for measurements in mouse tissues.

Extraction. As previously described⁴³, cecal, liver, human fecal samples (approximately 50 mg each), intact gallbladders and mouse portal veins were pre-weighed in lysis tubes containing ceramic beads (Precellys Lysing kit, tough micro-organism lysing VK05 tubes). Methanol (MeOH)-containing internal standard was added to cecal, liver, gallbladder, portal vein tissues and human feces. Tubes were homogenized in a MagNA Lyser. 50 μl of mouse serum and gallbladder contents were added to 50 μl of MeOH containing an internal standard. Cell culture medium was diluted 1:1 in MeOH. MeOH-extracted samples were centrifuged, diluted 1:1 in 50% MeOH:water, and injected into the UPLC–MS.

UPLC–MS analysis. BA profiling by UPLC–MS was performed using a published method⁴³. Total BAs in each sample were calculated by adding all detected and measured BAs. The limits of detection for individual BAs were determined using commercially available standards solubilized in 1:1 MeOH:water, and are as follows: CA7S, 0.05 pmol μl⁻¹; TγMCA, 0.01 pmol μl⁻¹; TDCA, 0.01 pmol μl⁻¹; LCA, 0.03 pmol μl⁻¹; isoLCA, 0.07 pmol μl⁻¹; 3-oxo-LCA, 0.05 pmol μl⁻¹; DCA, 0.04 pmol μl⁻¹; 3-oxo-CA, 0.04 pmol μl⁻¹; 3-oxo-CDCA, 0.4 pmol μl⁻¹; 7-oxo-CDCA, 0.03 pmol μl⁻¹; and 7-oxo-TCDDCA, 0.03 pmol μl⁻¹. The limits of detection of all other BAs have been reported previously⁴³. All standards were purchased from Sigma, Steraloids or Cayman Chemicals. CA7S and cholic acid-3-sulfate can be distinguished based on retention time using this UPLC–MS method.

Purification of CA7S. Extracted cecal contents from 11 SG mice (same as shown in Fig. 1) were pooled to provide sufficient material for purification. Pooled extract was purified via MS-guided HPLC of *m/z* 487 using a Luna RP C18

semi-preparative column, and water and acetonitrile with 0.1% formic acid as an additive.

NMR spectroscopy. CA7S and purified *m/z* 487 (<1 mg) were dissolved in 250 μl DMSO-d₆. NMR spectra were acquired on a Varian INOVA 500 MHz and are referenced internally according to residual solvent signals (DMSO to 2.50, HOD to 3.33).

Cell culture. NCI-H716 cells and Caco-2 cells were obtained from the American Type Culture Collection (ATCC). HEK293T cells from ATCC were a kind gift from the Blacklow lab (Department of Biological Chemistry and Molecular Pharmacology, HMS). Caco-2 and HEK293T cells were maintained in modified Eagle's medium (MEM) with GlutaMAX and Earle's Salts (Gibco, Life Technologies). NCI-H716 cells were maintained in RPMI 1640 with L-glutamine (GenClone). All cell culture media were supplemented with 10% fetal bovine serum (FBS), 100 units ml⁻¹ of penicillin and 100 μg ml⁻¹ of streptomycin (GenClone). Cells were grown in FBS- and antibiotic-supplemented 'complete' medium at 37 °C in an atmosphere of 5% CO₂. Testing of CA7S for agonist or antagonist activity against panels of 19 NHRs and 169 GPCRs was performed by DiscoverX (see Supplementary note for methods).

Caco-2 cell differentiation. Caco-2 cells were seeded in 24-well-plate transwells (0.4-μm pore size, Costar) at 200,000 cells per transwell. For apical/basolateral treatments, 200,000 Caco-2 cells were mixed with 50,000 NCI-H716 cells in six-well plate transwells (0.4-μm pore size, Costar) to mimic the ratio of epithelial cells to enteroendocrine cells in the human colon⁴⁴. The medium was changed on days 4, 8, 12, 16 and 18 to differentiate Caco-2 cells *in vitro*⁴⁵. On day 21, fully differentiated and polarized cells were validated for epithelial integrity by an FITC-D permeability assay before treatment with BAs.

In vitro BA treatments. NCI-H716 cells were seeded in cell culture plates coated with Matrigel (Corning Life Sciences, catalog no. 356234) diluted in Hanks' balanced salt solution (HBSS, Gibco) according to the manufacturer's instructions. The cells were allowed to grow for 2 d in complete RPMI medium. On the day of the treatment, cells were rinsed with low-serum (0.5% FBS) RPMI 1640 without antibiotics. BAs were diluted in DMSO (VWR International) and added to cells in the low-serum medium (0.5% FBS, RPMI 1640) without antibiotics. DMSO concentrations were constant throughout the treatments and used as a negative control. Differentiated Caco-2⁺ NCI-H716 cells were treated with BAs either apically or basolaterally in low-serum medium (0.5% FBS, RPMI 1640) without antibiotics. NCI-H716 cells were treated in suspension with BAs for *Tgr5* expression. After a 2-h incubation, medium was collected in tubes containing 0.1% trifluoroacetic acid (TFA, Sigma) in sterile water (GenClone). Cells used for GLP-1 measurements were treated with cold cell lysis solution (1% TFA, 1 M hydrochloric acid, 5% formic acid, 1% NaCl), scraped off the Matrigel and collected in lysing tubes. For calcium measurements, cells were collected in lysing tubes with PBS. Cells were lysed in a MagNA Lyser. Cells used for RNA extraction were treated with TRIzol (Ambion, Life Technologies, Thermo Fisher Scientific) and stored at –80 °C.

GLP-1 and insulin measurements. Total GLP-1 measurements were performed using the GLP-1 EIA Kit (Sigma, catalog no. RAB0201) and total insulin levels were measured using the Mouse Ins1/Insulin-1 ELISA kit (Sigma, catalog no. RAB0817). Mouse serum samples, NCI-H716 cell lysates and cells were stored at –80 °C and thawed on ice before performing assays. Then, 20 μl of the mouse serum samples were used directly in the GLP-1 ELISA assay, whereas 50 μl of the mouse serum samples were used directly in the insulin ELISA assay. Cell culture supernatant was directly used in the GLP-1 ELISA assay. Cell lysates were subjected to peptide purification using Sep Pak C18 Classic columns (Waters Corp.). The column was pretreated with a solution of 0.1% TFA in 80% isopropyl alcohol (EMD Millipore) and equilibrated with 0.1% TFA in water. Cell lysates were loaded on to the column and washed with 0.1% TFA in 80% isopropyl alcohol. The peptides were eluted in 0.1% TFA in water. The eluate was dried under vacuum and resuspended in 0.1% TFA in water. Total secreted (in medium) and intracellular (cell lysates) GLP-1 were calculated using the provided standard curve. Percentage GLP-1 secretion was calculated as follows:

$$\text{Percentage GLP-1 secretion} = \frac{\text{Total GLP-1 secreted (medium)}}{\text{Total GLP-1 secreted (medium)} + \text{Total GLP-1 in cell lysates}} \times 100.$$

The relative GLP-1 secretion was calculated compared with the DMSO control.

Plasmids and transient transfections. Human *Tgr5* was cloned using complementary DNA from human Caco-2 cells as a template, a forward primer with an *EcoRI* restriction site (5'-CGGAATTCGCACTTGGTCCTTGTGCTCT-3') and a reverse primer with a *XhoI* site (5'-GTCTCGAGTTAGTTCAAGTCCAGGTCGA-3'). The PCR product was cloned into the pCDNA3.1⁺ plasmid (Promega Corp.) and transfected at a concentration of 0.4 μg ml⁻¹ of medium. Endogenous FXR activation was assayed using a SHP-Luciferase reporter plasmid kindly gifted by K. Schoonjans (Ecole polytechnique fédérale de Lausanne, Switzerland). For luciferase reporter assays for

TGR5 activation, the CRE-driven luciferase construct pGL4.29[luc2P/CRE/Hygro] plasmid (Promega Corp.) and the pGL4.74[hRluc/CMV] plasmid (Promega Corp.) were used at a concentration of $2\ \mu\text{g ml}^{-1}$ and $0.05\ \mu\text{g ml}^{-1}$ of medium, respectively. For FXR activation, the SHP:Luciferase plasmid and the pGL4.74[hRluc/CMV] plasmid (Promega Corp.) were used at a concentration of $2\ \mu\text{g ml}^{-1}$ and $0.05\ \mu\text{g ml}^{-1}$ of medium, respectively. All plasmids were transfected using Opti-MEM (Gibco) and Lipofectamine 2000 (Invitrogen, Life Technologies). Transfections were performed in appropriate antibiotic-free medium with 10% FBS. After overnight incubation, BAs were added in complete medium, incubated overnight and harvested the next day for luciferase assay. *Tgr5* siRNA (Santa Cruz Biotechnology) and negative siRNA (Ambion) transfection was performed using Opti-MEM and Lipofectamine. The siRNAs were diluted in RNase-free water (Genesee) and added at a final concentration of 40 nM. After siRNA transfection, cells were incubated in antibiotic- and serum-free medium for 24 h and complete medium for an additional 24 h. BAs were then added (48 h post-siRNA transfection) in complete medium. After an overnight incubation, cells were harvested for luciferase assay or RNA extraction.

Luciferase reporter assay. Luminescence was measured using the Dual-Luciferase Reporter Assay System (Promega Corp.) according to the manufacturer's instructions. Cells were washed with PBS and lysed in passive lysis buffer from the kit. Matrigel-attached cells were scraped in passive lysis buffer. Luminescence was measured using the SpectraMax M5 plate reader (Molecular Devices) at the ICCB-Longwood Screening Facility at Harvard Medical School (HMS). Luminescence was normalized to *Renilla* luciferase activity.

Calcium measurement. CA7S-treated NCI-H716 cells collected in PBS were used to measure intracellular calcium using the Calcium Assay Kit (Fluorometric) (Abcam). Cell lysate supernatants were directly used in the calcium assay according to the manufacturer's instructions. Fluorescence was measured using the SpectraMax M5 plate reader (Molecular Devices) at the ICCB-Longwood Screening Facility at HMS.

Differentiated Caco-2 permeability assay. CA7S was added in PBS at the indicated concentrations to the apical chamber of the transwells containing differentiated Caco-2 cells and incubated for 12 h. Caco-2 epithelial integrity was assayed by measuring passive diffusion of 4-kDa FITC-D (Sigma Aldrich) added at a concentration of $5\ \mu\text{M}$ to the apical chamber into the basolateral chamber. Fluorescence was read on the basolateral side of the transwell system using a SpectraMax M5 plate reader (Molecular Devices) at the ICCB-Longwood Screening Facility at HMS.

Cell viability assay. Caco-2 cells were treated with CA7S diluted in DMSO in complete MEM. DMSO concentration was kept constant and used as a negative control. Cells were incubated with CA7S overnight at $37\ ^\circ\text{C}$ in a 5% CO_2 atmosphere. They were then treated with 0.25% trypsin in HBSS (GenClone) for 10 min at $37\ ^\circ\text{C}$. Cell viability was measured in a Countess II automated cell counter (Invitrogen).

The pH stability test. The stability of CA7S at physiological pH values was determined using the Waters' pH stability test. Buffers of pH 1 (0.1 M HCl), pH 7.4 (PBS) and pH 9 (10 mM ammonium formate solution adjusted to pH 9 with ammonium hydroxide) (all from Sigma) were prepared. CA7S was incubated in the pH buffers overnight at $37\ ^\circ\text{C}$ with gentle shaking (50g). CA7S solution was then diluted in MeOH and injected into the UPLC-MS.

RNA extraction and qPCR. Cells frozen in TRIzol (Ambion) were collected in RNase-free Eppendorf tubes and vortexed. Tissues were collected in tubes with TRIzol, followed by homogenization in a MagNA Lyser (Roche). Differentiated cells in transwells were scraped and collected in tubes. Tubes were kept on ice whenever possible. Total RNA was extracted by chloroform partitioning of RNA into the aqueous supernatant, followed by 2-propanol precipitation and 70% ethanol washing of the RNA pellet. The RNA pellet was air dried and resuspended in RNase-free H_2O (GenClone). Then, cDNA synthesis was performed using the High Capacity cDNA Reverse Transcription Kit (Applied Biosystems, Invitrogen). Quantitative (q)PCR was performed using the LightCycler 480 SYBR Green I Mater (Roche) in a 384-well format using the LightCycler 480 System (Roche) or the QuantStudio 7 (Thermo Fisher Scientific) at the ICCB-Longwood Screening Facility at HMS. Cq values >45 were considered to be not detected. The $2^{-\Delta\Delta\text{Ct}}$ method was used to calculate the relative gene expression change. Human *Tgr5* gene expression was normalized to the human *HPRT1* (*HGPRT*). Mouse *Glp1r* and *Tgr5* gene expression was normalized to 18S. Primer sequences were:

Human *Tgr5*: forward: 5'-CCTAGGAAGTGCCAGTGCAG-3',

reverse: 5'-CTTGGGTGGTAGGCAATGCT-3'; human *HGPRT*: forward: 5'-CCTGGCGTCGTGATTAGTGA-3',

reverse: 5'-CGAGCAAGACGTTCCAGTCT-3'; mouse

Glp1r: forward: 5'-AGGGCTTGATGGTGGCTATC-3',

reverse: 5'-GGACACTTAGGGGGCTTCAT-3';

Tgr5: forward: 5'-TTCTCTCTGTCCCGTGTG-3',

reverse: 5'-GGTGCTGCCAATGAGATGA-3'; mouse 18S:

forward: 5'-ATTGGAGCTGGAATTACCGC-3', reverse:

5'-CGGCTACCACATCCAAGGAA-3'.

In vivo enteral treatment with CA7S. The 13-week-old male DIO mice were purchased and housed as described in Animals. Mice were weight matched into two groups ($P=0.88$). After an overnight fast (17:00 to 07:00), mice received either CA7S or PBS via direct duodenal and rectal administration. The optimal, physiological dose of CA7S was extrapolated from the average picomolar concentration of CA7S in cecal samples from SG animals (average of 3,000 pmol per mg of stool with 500 mg stool per animal corresponding to 0.75 mg CA7S per cecum).

Under isoflurane general anesthesia, 0.25 mg and 0.75 mg CA7S in PBS, pH 7.2 was delivered by slow infusion (5 min) anterogradely into the duodenum and retrogradely into the rectum, respectively. The total volume of instillation was 2 ml ($0.5\ \text{mg CA7S ml}^{-1}$). Control animals received similar volumes of PBS alone. Then, 15 min post-infusion, serum glucose was measured via the tail vein followed by whole-blood collection via cardiac puncture into K^+ ethylenediaminetetraacetate tubes containing a dipeptidyl peptidase IV inhibitor (Merck Millipore), Perfabloc (Sigma) and apoprotinin (Sigma). One glucose reading from the PBS group was occluded by a clot, so it was excluded from glucose analysis. Whole blood and tissues were harvested for analysis. To account for changes in fasting times and hormonal diurnal rhythms, this experiment was carried out on 4 consecutive days such that only four mice were tested per day.

In vivo acute CA7S gavage. The 16-week-old DIO mice were purchased and housed as described in Animals. Mice were fasted for 4 h on the day of the experiment. Mice were orally gavaged with $100\ \text{mg kg}^{-1}$ of CA7S from $20\ \text{mg ml}^{-1}$ of solution, or an equivalent volume of PBS; 5 h after administration, whole blood and tissues were collected in the fasted state. One liver sample from the CA7S group was lost during sample preparation, so it was excluded from the BA analysis.

In vivo CA7S and OGTT. The 16-week-old DIO mice were purchased and housed as described in Animals. Blood glucose levels were monitored until average fasting glucose levels were $>160\ \text{mg dl}^{-1}$. Animals were fasted for 4 h on the day of the experiment. Mice were matched into two groups based on fasting glucose levels and received either $100\ \text{mg kg}^{-1}$ of CA7S from $20\ \text{mg ml}^{-1}$ of solution or an equivalent volume of PBS by oral gavage. After 3 h, an OGTT was performed using an oral gavage of $2\ \text{mg g}^{-1}$ of oral D-glucose (Sigma-Aldrich). Serum glucose was measured at baseline and at 15, 30, 60 and 120 min with a OneTouch glucometer.

Lentiviral IP injection. *Glp1r* and *Tgr5* shRNA-containing lentiviral particles (LVPs) were purchased from the MISSION TRC library (Sigma-Aldrich). LVPs containing a mixture of three *Glp1r* shRNA plasmid clones (TRCN0000004629, TRCN0000004630 and TRCN0000004633) and *Tgr5* shRNA plasmid clones (TRCN0000026777, TRCN0000026783 and TRCN0000026817) were purchased. Mice were maintained on an HFD until average fasting glucose $>160\ \text{mg dl}^{-1}$ in a BL2 facility. Under sterile conditions, mice were injected intraperitoneally with 0.2 ml of 5×10^5 shRNA LVPS^{46,47}. Then, 72 h after injection, mice underwent CA7S/PBS gavage followed by an OGTT as above. After completion of the the OGTT, mice were euthanized and their tissues harvested. *Glp1r* and *Tgr5* knockdown efficiency was measured in tissues by qPCR as described in RNA extraction and qPCR.

CA7S chronic feeding. The 16-week-old DIO mice were purchased and housed as described in Animals. Mice were orally gavaged daily for 48 d with $100\ \text{mg kg}^{-1}$ of CA7S or equivalent volume of PBS. Weight and food intake were measured daily. Both groups of mice exhibited initial weight loss during the experiment, presumably due to the stress of daily gavage. Mice were fasted overnight before euthanization. Fasting glucose was measured at euthanization. Whole blood and tissues were collected. Two gallbladders in the CA7S group perforated before weighing and were therefore excluded from the analysis. One liver sample from the CA7S group was lost after harvest and was thus not included in the analysis.

Human stool collection. After obtaining institutional review board approval and informed consent, we prospectively collected stool specimens from obese humans undergoing SG. Patients were selected randomly over the course of a 1-year enrollment with the following exclusion criteria: (1) antibiotic use within 3 months of surgery, (2) on immunosuppressants, (3) pre-existing immunocompromised state, (4) chronic diarrhea, (5) ulcerative colitis or Crohn's disease and (6) prior colon resection. For each patient, a preoperative stool specimen collected on the day of surgery was compared with a stool specimen obtained from PODs 14–99 (mode 15 d; median 36 d). Specimens were snap frozen in liquid nitrogen and stored at $-80\ ^\circ\text{C}$ until the BA analysis was performed by a blinded investigator.

Ethics. All mouse experiments were performed under the approval of the Brigham and Women's Hospital (BWH) Institutional Animal Care and Use Committee. Human stool collection was performed under the approval of the BWH Institutional Review Board.

Statistics and reproducibility. No statistical methods were used to predetermine sample size. Sample sizes were determined by magnitude and consistency of measurable differences. Statistical tests used for each experiment are outlined in the figure legends. All data are presented as mean \pm s.e.m. All in vitro studies represented in the article were performed in at least three biological replicates. Each experiment was reproduced in triplicate at least twice with similar results. In vivo mouse studies: the SG model is well established in the Sheu lab. The functional glucose data (IPGTT and ITT) are in keeping with previously published data from other labs^{6,48}. Thus, the number of mice used was kept to a minimum and replicate testing was not performed for the sham and SG surgeries. Bile acids were analyzed from four independently performed sham and SG surgeries over the course of a year, and the data represent all the replicates. CA7S enteral administration was not replicated owing to the clear significance of the results. CA7S acute gavage was performed in two independent experiments with similar results. The lentiviral knockdown experiments were performed in two independent experiments with similar results. The results of the chronic dosing experiment (Fig. 6) were reproduced in an independent cohort of mice ($n=7$) dosed with higher concentrations of CA7S. The present study includes three mouse studies (see Figs. 4, 5 and 6) which were performed by three different investigators (D.A.H., H.A. and J.L., respectively) at different times, thereby providing reproducible corroboration that CA7S remains gut restricted and improves hyperglycemia. Human stool samples from bariatric surgery patients were a scarce resource. We used all available samples and as such did not have samples available for replicate experiments. P values <0.05 were considered significant. Unless stated otherwise, the experiments were not randomized, and investigators were not blinded to allocation during in vitro and in vivo experiments.

Software. GraphPad Prism v.8 software was used to plot data and perform statistical analyses. ChemDraw software v.12 was used to draw chemical structures.

Reporting summary. Further information on research design is available in the Nature Research Reporting Summary linked to this article.

Data availability

All data generated or analyzed during this study are included in this article and its Supplementary information and extended data files.

Code availability

No custom code or mathematical algorithms were used in this study.

References

43. Yao, L. et al. A selective gut bacterial bile salt hydrolase alters host metabolism. *eLife* **7**, e37182 (2018).
44. Cristina, M. L., Lehy, T., Zeitoun, P. & Dufougeray, F. Fine structural classification and comparative distribution of endocrine cells in normal human large intestine. *Gastroenterology* **75**, 20–28 (1978).
45. Verhoeckx, K. et al. Caco-2 cell line. *Impact Food Bioact. Health* **175**, 103–111 (2015).

46. Tiscornia, G., Singer, O., Ikawa, M. & Verma, I. M. A general method for gene knockdown in mice by using lentiviral vectors expressing small interfering RNA. *Proc. Natl Acad. Sci. USA* **100**, 1844–1848 (2003).
47. Blosser, W. et al. A method to assess target gene involvement in angiogenesis in vitro and in vivo using lentiviral vectors expressing shRNA. *PLoS ONE* **9**, e96036 (2014).
48. Abu-Gazala, S. et al. Sleeve gastrectomy improves glycemia independent of weight loss by restoring hepatic insulin sensitivity. *Diabetes* **67**, 1079–1085 (2018).

Acknowledgements

We thank members of the Devlin, Sheu, Clardy and Banks labs (HMS) for helpful discussions and advice. We would like to acknowledge the Blacklow and Kruse labs for help with equipment and reagents, and the BWH mouse facility. We would like to thank K. Schoonjans (Ecole polytechnique fédérale de Lausanne) for the FXR reporter plasmid. We thank the human patients who participated in the present study. This work was supported by a KL2 award from Harvard Catalyst (no. 4KL2TR001100-04 to E.G.S.), a pilot grant from Boston Area Diabetes and Endocrinology Research Center (BADERC) (no. NIH/NIDDK P30 DK057521 to E.G.S.), an NIH MIRA grant (no. R35 GM128618 to A.S.D.), a Blavatnik Biomedical Accelerator at Harvard University grant (to A.S.D.), a Quadrangle Fund for the Advancement and Seeding of Translational Research at Harvard Medical School (Q-FASTR) grant (to A.S.D. and E.G.S.), an American Heart Association Postdoctoral Fellowship (to S.N.C.), a HMS Department of Biological Chemistry and Molecular Pharmacology Fellowship (to S.N.C.), an American College of Surgeons fellowship (to D.A.H.), an NIH T32 training grant (to D.A.H. and J.N.L.), and a DRC P&F program grant from the Joslin Diabetes Center (no. P30DK036836) (to A.H.V.).

Author contributions

A.S.D., E.G.S., S.N.C. and D.A.H. conceived the project and designed the experiments. S.N.C. performed the cell culture experiments, BA profiling, and transcriptional analyses and hormone quantifications on mouse tissues and blood. D.A.H. performed the mouse surgeries and the enteral administration in vivo experiments. H.A., R.S. and J.N.L. performed the gavages, OGTs and lentiviral injection experiments. J.N.L. performed the chronic dosing experiments. M.T.H. performed NMR analyses. A.H.V. collected and provided the human samples. S.N.C., D.A.H., E.G.S. and A.S.D. wrote the manuscript. A.T. provided feedback and reviewed the manuscript. All authors edited and contributed to the critical review of the manuscript.

Competing interests

CA7S is a subject of patents held by HMS and BWH on which S.N.C., D.A.H., E.G.S. and A.S.D. are inventors. A.S.D. is a consultant for Kintai Therapeutics and HP Hood. E.G.S. was previously on the scientific advisory board of Kitotech, Inc.

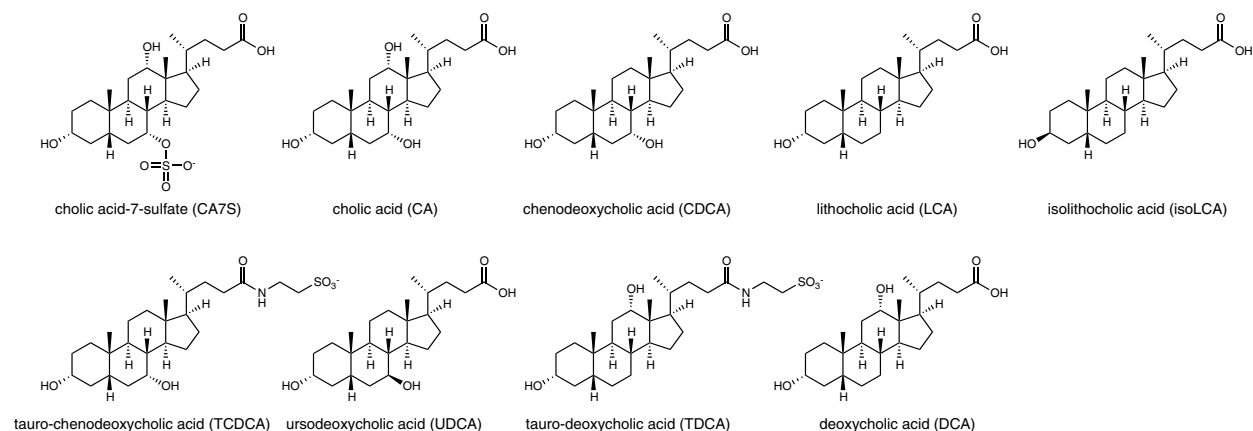
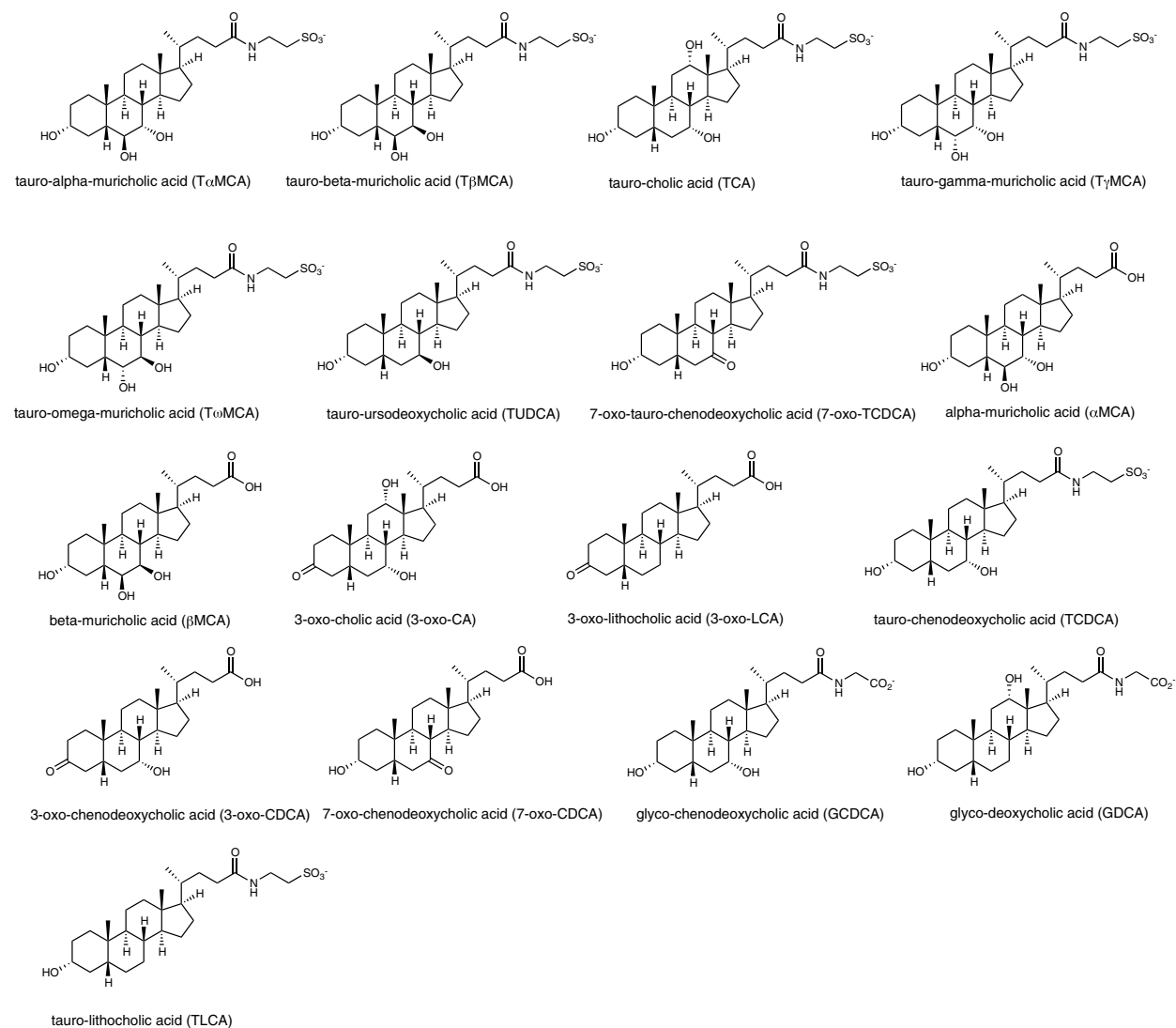
Additional information

Extended data is available for this paper at <https://doi.org/10.1038/s41589-020-0604-z>.

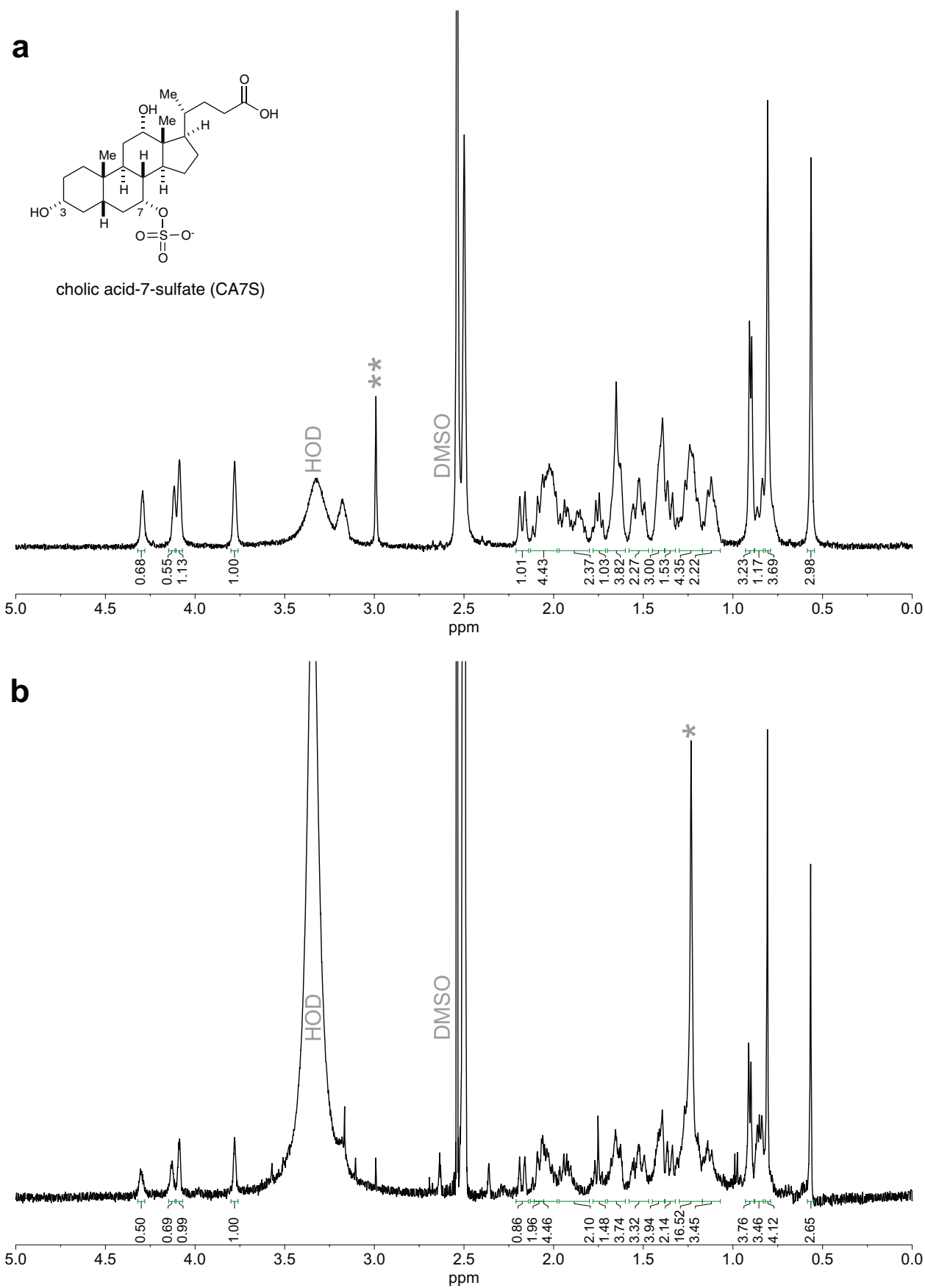
Supplementary information is available for this paper at <https://doi.org/10.1038/s41589-020-0604-z>.

Correspondence and requests for materials should be addressed to E.G.S. or A.S.D.

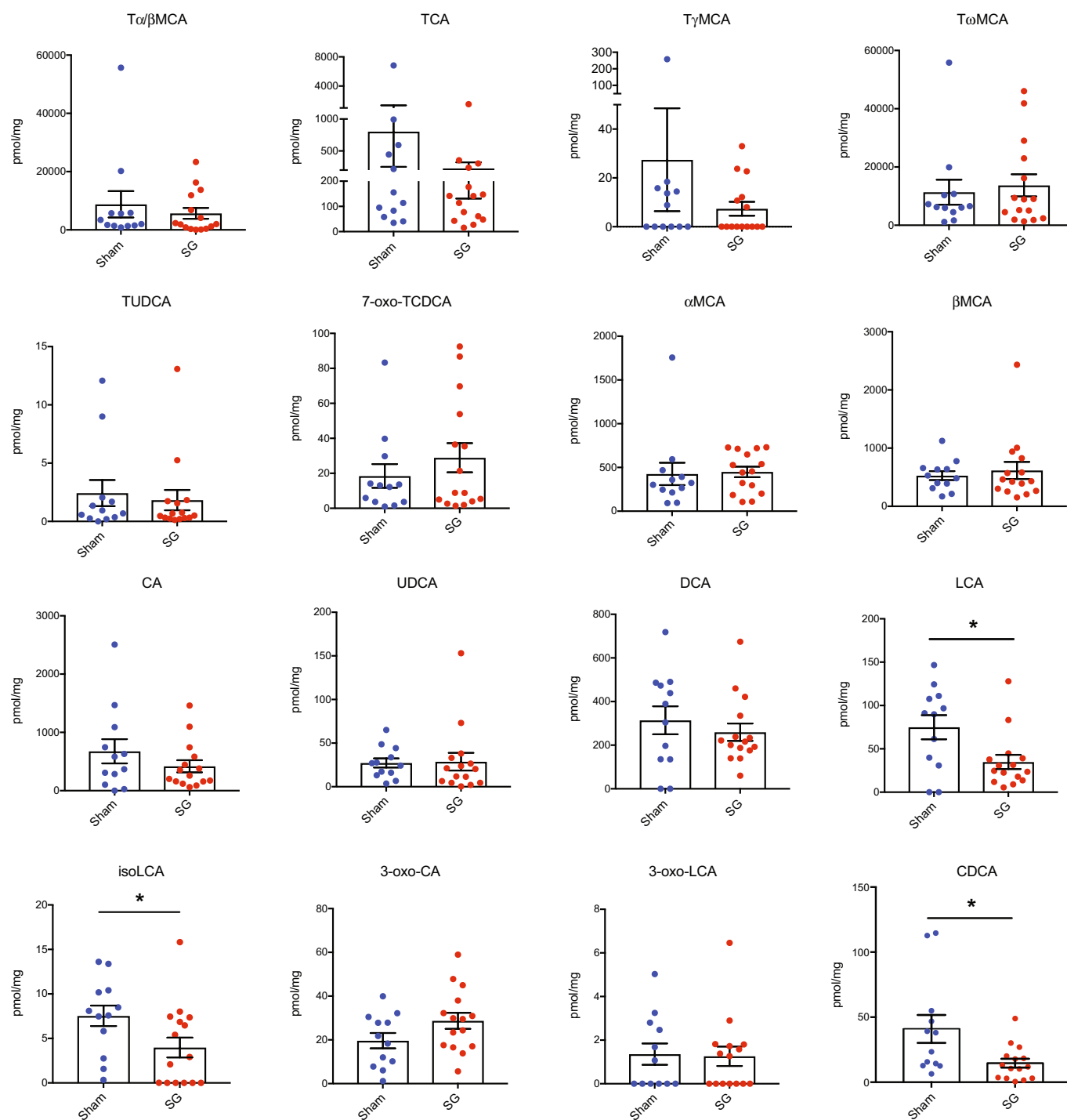
Reprints and permissions information is available at www.nature.com/reprints.

a**b**

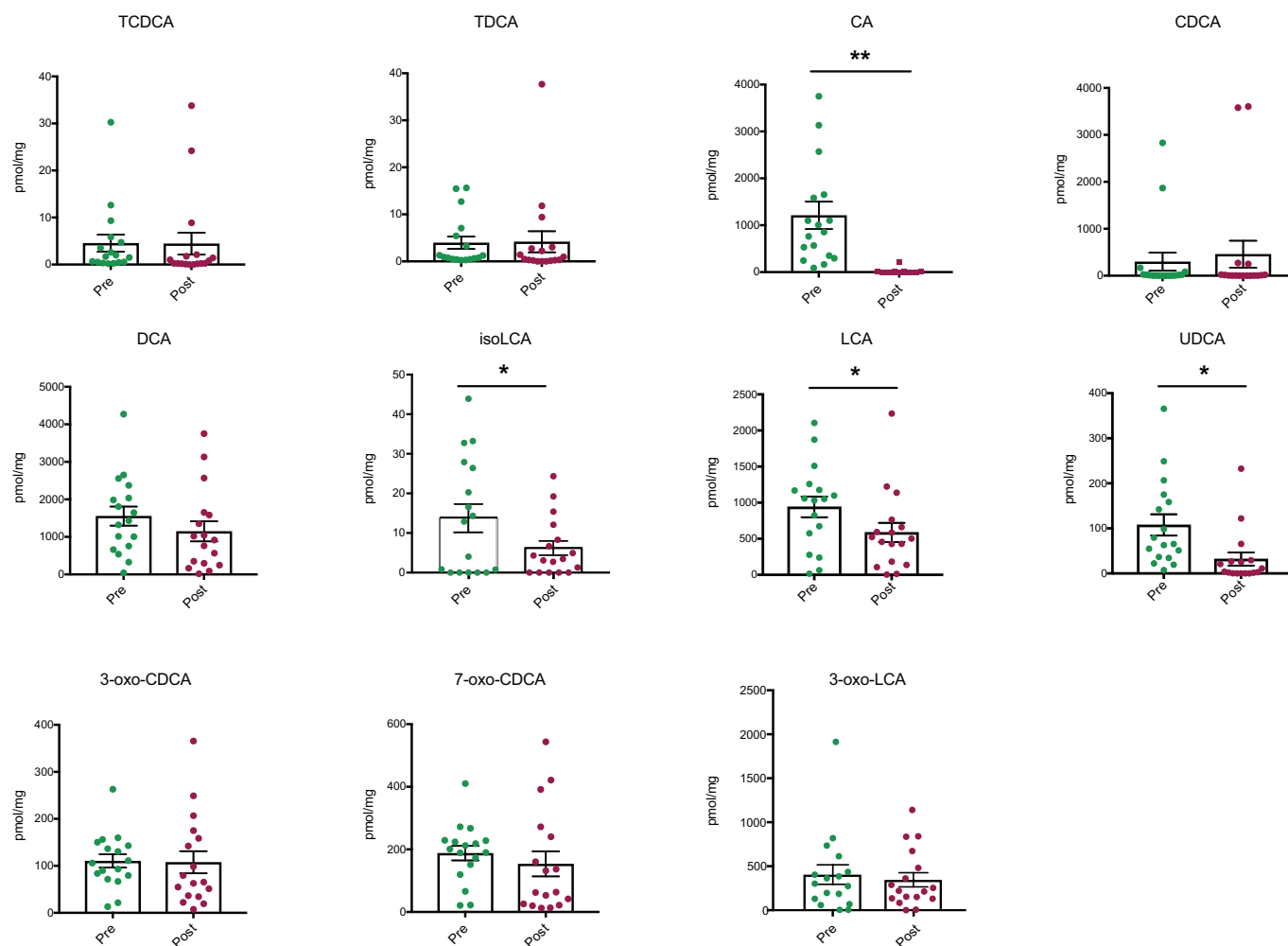
Extended Data Fig. 1 | Bile acid structures. **a**, Structures of bile acids in main text and figures. **b**, Structures of additional bile acids in Extended Data and Supplementary Information.



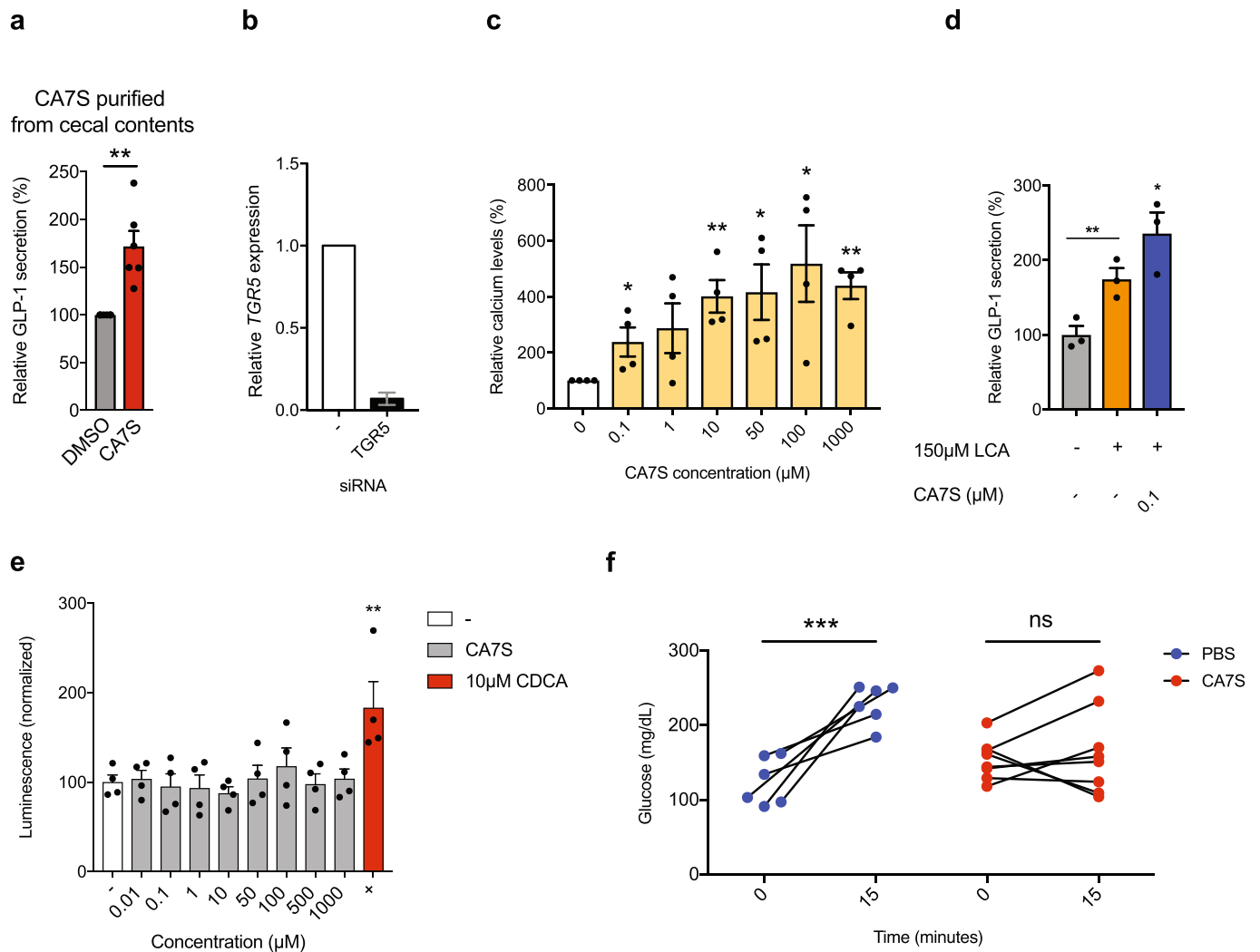
Extended Data Fig. 2 | NMR of cholic acid-7-sulfate. a, ^1H NMR of authentic sample of cholic acid-7-sulfate (CA7S) (Cayman Chemical). **b,** ^1H NMR of CA7S purified from the cecal contents of SG mice. Signals between 3.7 to 4.4 ppm are diagnostic of CA7S. Impurities are denoted by asterisks.



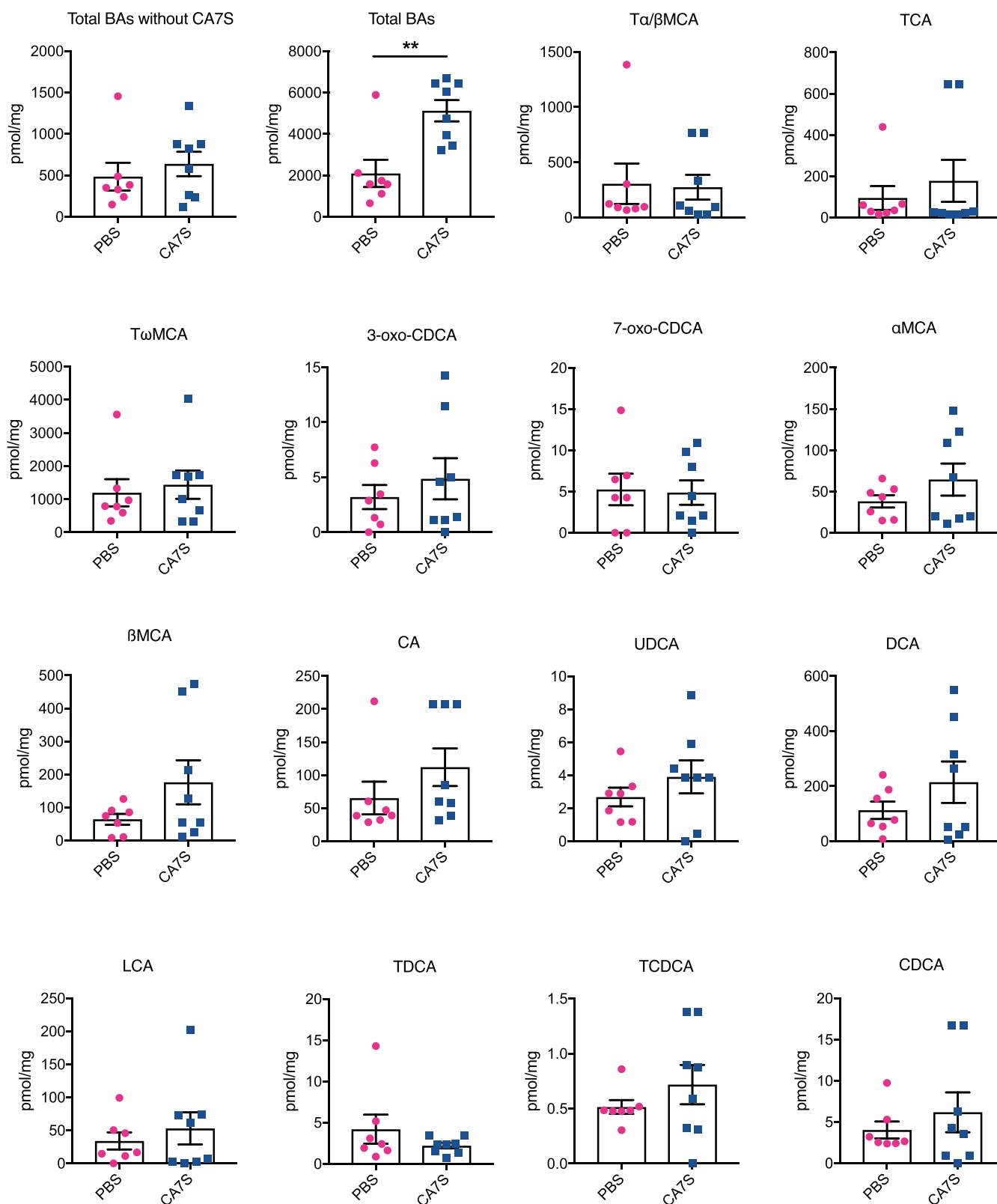
Extended Data Fig. 3 | Bile acid concentrations in cecal contents of mice post-sham or post-SG. Six weeks following surgery, cecal contents were collected from sham or SG mice after an overnight fast. Bile acids were quantified using UPLC-MS (sham, $n=12$, SG, $n=15$, data not marked with asterisk(s) are not significant). All bile acids with measurable concentrations above the limit of detection are shown. T α / β MCA, tauro-alpha- and tauro-beta-muricholic acid, $p=0.53$; TCA, tauro-cholic acid, $p=0.32$; T γ MCA, tauro-gamma-muricholic acid, $p=0.36$; T ω MCA, tauro-omega-muricholic acid, $p=0.68$; TUDCA, tauro-ursodeoxycholic acid, $p=0.67$; 7-oxo-TCDC, 7-oxo-tauro-chenodeoxycholic acid $p=0.34$; α MCA, alpha-muricholic acid, $p=0.87$; β MCA, beta-muricholic acid, $p=0.59$; CA, cholic acid, $p=0.28$; UDCA, ursodeoxycholic acid, $p=0.85$; DCA, deoxycholic acid, $p=0.48$; LCA, lithocholic acid, $*p=0.02$; isoLCA, isolithocholic acid $*p=0.02$; 3-oxo-CA, 3-oxo-cholic acid, $p=0.08$; 3-oxo-LCA, 3-oxo-lithocholic acid, $p=0.79$; CDCA, chenodeoxycholic acid, $*p=0.03$, two-tailed Welch's t -test. All data are presented as mean \pm SEM.



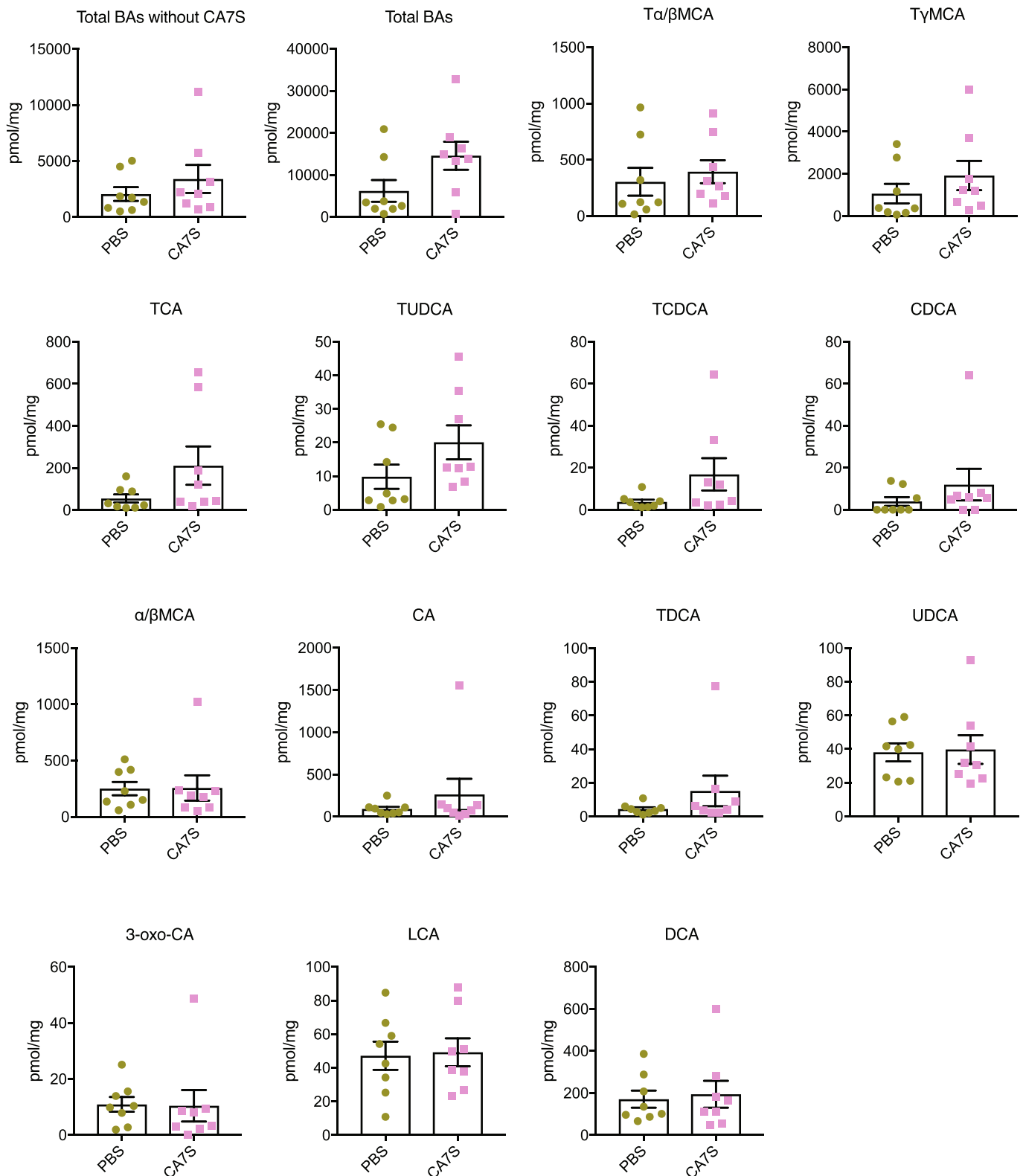
Extended Data Fig. 4 | Bile acid concentrations in feces of human patients pre-SG or post-SG. Feces were collected from patients pre-op or -5 weeks post-op and bile acids were quantified using UPLC-MS ($n=17$ patients, median 36 days after surgery, data not marked with asterisk(s) are not significant). All bile acids with measurable concentrations above the limit of detection are shown. TCDCA, tauro-chenodeoxycholic acid, $p=0.97$; TDCA, tauro-deoxycholic acid, $p=0.93$; CA, cholic acid, $**p=1.00\times 10^{-3}$; CDCA, chenodeoxycholic acid, $p=0.52$; DCA, deoxycholic acid, $p=0.13$; LCA, lithocholic acid, $*p=0.01$; isoLCA, iso-lithocholic acid, $*p=0.03$; UDCA, ursodeoxycholic acid, $*p=0.02$; 3-oxo-CDCA, 3-oxo-chenodeoxycholic acid, $p=0.92$; 7-oxo-CDCA, 7-oxo-chenodeoxycholic acid, $p=0.47$; 3-oxo-LCA, 3-oxo-lithocholic acid, $p=0.56$, two-tailed paired t-test. All data are presented as mean \pm SEM.



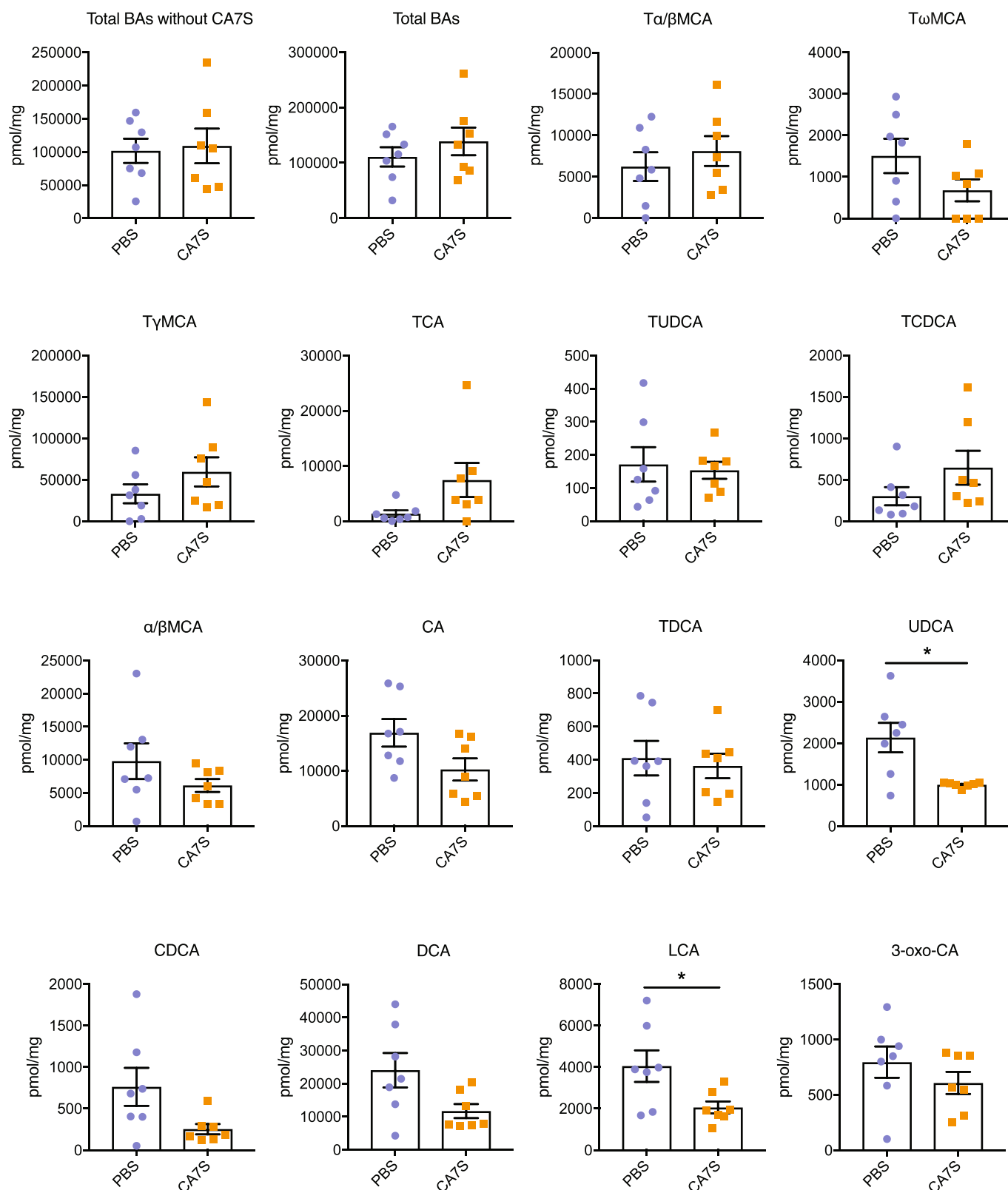
Extended Data Fig. 5 | CA7S agonizes TGR5 but not FXR, induces GLP-1 secretion, and reduces systemic glucose levels. **a**, CA7S (500 μM) purified from SG mouse cecal contents induced secretion of GLP-1 in NCI-H716 cells compared to DMSO control (6 biological replicates per condition, $**p=1.00 \times 10^{-3}$, two-tailed Welch's t-test). **b**, Quantitative real time PCR analysis of expression of human *TGR5* in *TGR5* siRNA and negative (-) siRNA-treated NCI-H716 cells for Fig. 3b. **c**, CA7S induced an increase in intracellular calcium levels in NCI-H716 cells (4 biological replicates per condition, CA7S 10 μM $*p=0.03$, 50 μM $*p=0.02$, 100 μM $**p=1.80 \times 10^{-3}$, 100 μM $*p=0.01$, one-way ANOVA followed by Dunnett's multiple comparisons test). **d**, CA7S induced secretion of GLP-1 in the presence of a physiologically relevant concentration of LCA (150 μM) (3 biological replicates per condition, DMSO (-) control vs. LCA $**p=9.90 \times 10^{-3}$, CA7S vs. LCA 0.1 μM $*p=0.03$, two-way ANOVA followed by Dunnett's multiple comparisons test). **e**, CA7S did not induce activation of endogenous FXR in Caco-2 cells compared to (-) DMSO control. Known FXR agonist CDCA (10 μM) was used as a positive control (4 biological replicates per condition, CA7S 0.01-50 μM and 500-1000 μM not significant $p=0.99$, CA7S 100 μM not significant $p=0.96$, CDCA 10 μM $**p=4.60 \times 10^{-3}$, one-way ANOVA followed by Dunnett's multiple comparisons test). **f**, In vivo change in serum glucose upon acute enteral treatment with PBS and CA7S (PBS, $n=6$; CA7S, $n=8$ mice, $**p=1.00 \times 10^{-4}$, ns=not significant $p=0.63$, two-tailed paired t-test). All data are presented as mean \pm SEM.



Extended Data Fig. 6 | Bile acid concentrations in cecal contents of mice treated enterally with CA7S. Cecal contents were collected from mice after enteral treatment with CA7S or PBS and bile acids were quantified using UPLC-MS (PBS, $n=7$, CA7S, $n=8$, data not marked with asterisk(s) are not significant). All bile acids with measurable concentrations above the limit of detection are shown. Total BAs without CA7S, $p=0.50$; Total bile acids (BAs), $**p=3.5 \times 10^{-3}$; T α / β MCA, tauro- α - and tauro- β -muricholic acid, $p=0.88$; TCA, tauro- α -cholic acid, $p=0.49$; T ω MCA, tauro- ω -muricholic acid, $p=0.68$; 3-oxo-CDCA, 3-oxo-chenodeoxycholic acid $p=0.45$; 7-oxo-CDCA, 7-oxo-chenodeoxycholic acid $p=0.87$; α MCA, α -muricholic acid, $p=0.23$; β MCA, β -muricholic acid, $p=0.14$; CA, cholic acid, $p=0.23$; UDCA, ursodeoxycholic acid, $p=0.30$; DCA, deoxycholic acid, $p=0.24$; LCA, lithocholic acid, $p=0.50$; TDCA, tauro-deoxycholic acid, $p=0.30$; TCDCA, tauro-chenodeoxycholic acid, $p=0.31$; CDCA, chenodeoxycholic acid, $p=0.43$, two-tailed Welch's t -test. All data are presented as mean \pm SEM.



Extended Data Fig. 7 | Bile acid concentrations in cecal contents of mice gavaged with one dose of CA7S. Fasted DIO mice were gavaged with CA7S or PBS and cecal contents were collected from mice 5 hours post-gavage. Bile acids were quantified using UPLC-MS ($n=8$ in each group, data not marked with asterisk(s) are not significant). All bile acids with measurable concentrations above the limit of detection are shown. Total BAs without CA7S, $p=0.35$; Total bile acids (BAs), $p=0.06$; T α / β MCA, tauro-alpha- and tauro-beta-muricholic acid, $p=0.58$; T γ MCA, tauro-gamma-muricholic acid, $p=0.32$; TCA, tauro-cholic acid, $p=0.13$; TUDCA, tauro-ursodeoxycholic acid, $p=0.12$; TCDCA, tauro-chenodeoxycholic acid, $p=0.13$; CDCA, chenodeoxycholic acid, $p=0.33$; α / β MCA, alpha-muricholic acid and beta-muricholic acid, $p=0.96$; CA, cholic acid, $p=0.38$; TDCA, tauro-deoxycholic acid, $p=0.27$; UDCA, ursodeoxycholic acid, $p=0.87$; 3-oxo-CA, 3-oxo-cholic acid, $p=0.93$; LCA, lithocholic acid, $p=0.86$; DCA, deoxycholic acid, $p=0.76$, two-tailed Welch's t-test. All data are presented as mean \pm SEM.



Extended Data Fig. 8 | Bile acid concentrations in cecal contents of mice gavaged chronically with CA7S. Cecal contents were collected from mice following an overnight fast after 48 days of daily gavage with CA7S or PBS. Bile acids were quantified using UPLC-MS ($n = 7$ in each group, data not marked with asterisk(s) are not significant). All bile acids with measurable concentrations above the limit of detection are shown. Total BAs without CA7S, $p = 0.82$; Total bile acids (BAs), $p = 0.38$; T α / β MCA, tauro-alpha- and tauro-beta-muricholic acid, $p = 0.46$; T ω MCA, tauro-omega-muricholic acid, $p = 0.12$; T γ MCA, tauro-gamma-muricholic acid, $p = 0.23$; TCA, tauro-cholic acid, $p = 0.09$; TUDCA, tauro-ursodeoxycholic acid, $p = 0.76$; TCDCa, tauro-chenodeoxycholic acid, $p = 0.17$; α / β MCA, alpha-muricholic acid and beta-muricholic acid, $p = 0.23$; CA, cholic acid, $p = 0.06$; TDCA, tauro-deoxycholic acid, $p = 0.71$; UDCA, ursodeoxycholic acid, $*p = 0.01$; CDCA, chenodeoxycholic acid, $p = 0.06$; DCA, deoxycholic acid, $p = 0.23$; LCA, lithocholic acid, $*p = 0.04$; 3-oxo-CA, 3-oxo-cholic acid, $p = 0.30$, two-tailed Welch's t-test. All data are presented as mean \pm SEM.

Reporting Summary

Nature Research wishes to improve the reproducibility of the work that we publish. This form provides structure for consistency and transparency in reporting. For further information on Nature Research policies, see [Authors & Referees](#) and the [Editorial Policy Checklist](#).

Statistics

For all statistical analyses, confirm that the following items are present in the figure legend, table legend, main text, or Methods section.

n/a Confirmed

- | | | |
|-------------------------------------|-------------------------------------|--|
| <input type="checkbox"/> | <input checked="" type="checkbox"/> | The exact sample size (n) for each experimental group/condition, given as a discrete number and unit of measurement |
| <input type="checkbox"/> | <input checked="" type="checkbox"/> | A statement on whether measurements were taken from distinct samples or whether the same sample was measured repeatedly |
| <input type="checkbox"/> | <input checked="" type="checkbox"/> | The statistical test(s) used AND whether they are one- or two-sided
<i>Only common tests should be described solely by name; describe more complex techniques in the Methods section.</i> |
| <input checked="" type="checkbox"/> | <input type="checkbox"/> | A description of all covariates tested |
| <input type="checkbox"/> | <input checked="" type="checkbox"/> | A description of any assumptions or corrections, such as tests of normality and adjustment for multiple comparisons |
| <input type="checkbox"/> | <input checked="" type="checkbox"/> | A full description of the statistical parameters including central tendency (e.g. means) or other basic estimates (e.g. regression coefficient) AND variation (e.g. standard deviation) or associated estimates of uncertainty (e.g. confidence intervals) |
| <input type="checkbox"/> | <input checked="" type="checkbox"/> | For null hypothesis testing, the test statistic (e.g. F , t , r) with confidence intervals, effect sizes, degrees of freedom and P value noted
<i>Give P values as exact values whenever suitable.</i> |
| <input checked="" type="checkbox"/> | <input type="checkbox"/> | For Bayesian analysis, information on the choice of priors and Markov chain Monte Carlo settings |
| <input checked="" type="checkbox"/> | <input type="checkbox"/> | For hierarchical and complex designs, identification of the appropriate level for tests and full reporting of outcomes |
| <input checked="" type="checkbox"/> | <input type="checkbox"/> | Estimates of effect sizes (e.g. Cohen's d , Pearson's r), indicating how they were calculated |

Our web collection on [statistics for biologists](#) contains articles on many of the points above.

Software and code

Policy information about [availability of computer code](#)

Data collection

No software was used for the collection of in vivo data

Data analysis

GraphPad Prism (version 8) software was used to plot data and perform statistical analyses. ChemDraw software (version 12) was used to draw chemical structures.

For manuscripts utilizing custom algorithms or software that are central to the research but not yet described in published literature, software must be made available to editors/reviewers. We strongly encourage code deposition in a community repository (e.g. GitHub). See the Nature Research [guidelines for submitting code & software](#) for further information.

Data

Policy information about [availability of data](#)

All manuscripts must include a [data availability statement](#). This statement should provide the following information, where applicable:

- Accession codes, unique identifiers, or web links for publicly available datasets
- A list of figures that have associated raw data
- A description of any restrictions on data availability

All data generated or analyzed during this study are included in this article and its supplementary information and extended data files.

Field-specific reporting

Please select the one below that is the best fit for your research. If you are not sure, read the appropriate sections before making your selection.

Life sciences Behavioural & social sciences Ecological, evolutionary & environmental sciences

For a reference copy of the document with all sections, see [nature.com/documents/nr-reporting-summary-flat.pdf](https://www.nature.com/documents/nr-reporting-summary-flat.pdf)

Life sciences study design

All studies must disclose on these points even when the disclosure is negative.

Sample size

Sample sizes for in vitro experiments are fully disclosed in the manuscript. For in vitro and in vivo experiments, no statistical methods were used to predetermine sample size. Sample sizes were determined by magnitude and consistency of measurable differences. Every in vitro study was performed in at least 3 biological replicates and reproduced with similar results at least twice. The number of technical replicates were determined according to manufacturer's instructions for data acquisition.

In vivo mouse studies: A sample size determination was not completed. However, the Sheu lab has expertise in bariatric surgical models in mice and based on our prior work (Harris et al; Subramaniam et. al) , a sample size was selected such that we used the maximum number of mice that could be cared for while allowing determination of clear statistical significance. Our sample size is in keeping with previously published studies. (Ryan et. al., Wilson-Pérez et al) CA75 enteral administration, and acute and chronic gavage studies were performed on 13-16 week old mice. Again a sample size determination was not completed but we maximized the number of mice that could be cared for during the experiment in order to achieve the highest statistical power.

Lentiviral knockdown experiments: The appropriate dose of lentiviral particle injection for efficient knockdown was worked out in pilot experiments. A similar number of animals were chosen as stated above for CA75 in vivo experiments.

- Harris DA, Mina A, Cabarkapa D, et al. Sleeve Gastrectomy enhances glucose utilization and remodels adipose tissue independent of weight loss. *Am J Physiol Endocrinol Metab.* February 2020. doi:10.1152/ajpendo.00441.2019.
 - Ryan KK, Tremaroli V, Clemmensen C, et al. FXR is a molecular target for the effects of vertical sleeve gastrectomy. *Nature.* 2014;509(7499):183-188. doi:10.1038/nature13135
 - Subramaniam R, Aliakbarian H, Bhutta HY, Harris DA, Tavakkoli A, Sheu EG. Sleeve Gastrectomy and Roux-en-Y Gastric Bypass Attenuate Pro-inflammatory Small Intestinal Cytokine Signatures. *Obesity surgery.* July 2019:1-9. doi:10.1007/s11695-019-04059-0.
 - Wilson-Pérez HE, Chambers AP, Ryan KK, et al. Vertical sleeve gastrectomy is effective in two genetic mouse models of glucagon-like Peptide 1 receptor deficiency. *Diabetes.* 2013;62(7):2380-2385. doi:10.2337/db12-1498.

Human samples: A sample size determination was not completed and we used the maximum number of patient samples that we had access to that had both pre- and post-operative stool samples.

Data exclusions

No data were excluded from the analyses

Replication

All in vitro studies represented in the publication were performed in at least 3 biological replicates. Each experiment was reproduced in triplicate at least twice with similar results.

In vivo mouse studies: The sleeve gastrectomy model is well established in the Sheu lab. The functional glucose data (IPGTT and ITT) is in keeping with previously published data from other labs. Thus, the number of mice used was kept to a minimum and replicate testing was not performed for the Sham and SG surgeries. Bile acid were analyzed from four independently performed Sham and SG surgeries over the course of a year, and the data in the manuscript represents all the replicates. CA75 enteral administration was not replicated owing to the clear significance of the results. CA75 acute gavage was performed in two independent experiments with similar results. The lentiviral knockdown experiments were performed in two independent experiments with similar results. The chronic dosing experiment (Fig. 6) results were reproduced in an independent cohort of mice (n=7) dosed with higher concentrations of CA75. The paper includes 3 mouse studies (Figs. 4, 5, 6) which were performed by 3 different investigators (D.A.H., H.A., J.L. respectively) at different times, thereby providing reproducible corroboration that CA75 remains gut-restricted and improves hyperglycemia.

Ryan KK, Tremaroli V, Clemmensen C, et al. FXR is a molecular target for the effects of vertical sleeve gastrectomy. *Nature.* 2014;509(7499):183-188. doi:10.1038/nature13135.
 Abu-Gazala S, Horwitz E, Ben-Haroush Schyr R, et al. Sleeve Gastrectomy Improves Glycemia Independent of Weight Loss by Restoring Hepatic Insulin Sensitivity. *Diabetes.* 2018;67(6):1079-1085. doi:10.2337/db17-1028.

Human stool samples from bariatric surgery patients were a scarce resource. We used all available samples and as such did not have samples available for replicate experiments.

Randomization

In vitro experiments were performed by splitting cells from the same flask to individual wells for treatments without bias.

In vivo mouse studies: Mice were matched into groups based on weight or fasting blood glucose where appropriate.

Human patients were selected randomly over the course of 1 year with the following exclusion criteria: 1) antibiotic use within 3 months of surgery, 2) on immunosuppressants, 3) pre-existing immunocompromised state, 4) chronic diarrhea, 5) Ulcerative colitis or Crohn's disease, 6)

prior colon resection. Samples were de-identified as per the IRB protocol, and bile acid analyses were performed by a blinded investigator. Covariates in this study were patient pre- and post-SG fecal samples, information used to perform two-tailed paired t-test statistical analyses

Blinding

Data from in vitro experiments were acquired from equipment capable of batch-analysis and were analyzed using computational softwares. This eliminated human error and bias, and thus we did not blind the data from investigators.

In vivo mouse studies: For surgical studies, due to the need for close post-operative monitoring, examiners were kept unblinded to the surgery performed on mice. For CA7S in vivo studies, operative instillation of CA7S or PBS was not done in blinded fashion in order to closely monitor the health of the animals. However, post-hoc analyses (of serum GLP1 and insulin, and CA7S analysis in tissues) were completed by a blinded, second experimenter.

Human studies: Patient samples were de-identified and BA analysis was completed in a blinded fashion.

Reporting for specific materials, systems and methods

We require information from authors about some types of materials, experimental systems and methods used in many studies. Here, indicate whether each material, system or method listed is relevant to your study. If you are not sure if a list item applies to your research, read the appropriate section before selecting a response.

Materials & experimental systems

n/a	Involvement
<input checked="" type="checkbox"/>	<input type="checkbox"/> Antibodies
<input type="checkbox"/>	<input checked="" type="checkbox"/> Eukaryotic cell lines
<input checked="" type="checkbox"/>	<input type="checkbox"/> Palaeontology
<input type="checkbox"/>	<input checked="" type="checkbox"/> Animals and other organisms
<input type="checkbox"/>	<input checked="" type="checkbox"/> Human research participants
<input checked="" type="checkbox"/>	<input type="checkbox"/> Clinical data

Methods

n/a	Involvement
<input checked="" type="checkbox"/>	<input type="checkbox"/> ChIP-seq
<input checked="" type="checkbox"/>	<input type="checkbox"/> Flow cytometry
<input checked="" type="checkbox"/>	<input type="checkbox"/> MRI-based neuroimaging

Eukaryotic cell lines

Policy information about [cell lines](#)

Cell line source(s)	Intestinally-derived human Caco-2 cell line and enteroendocrine human NCI-H716 cells line was obtained from ATCC; human embryonic kidney HEK293T cells from ATCC were a generous gift from the Blacklow lab at Harvard Medical School.
Authentication	None of the cell lines were authenticated
Mycoplasma contamination	Cell lines were not tested for mycoplasma contamination
Commonly misidentified lines (See ICLAC register)	No misidentified cell lines were used in this study

Animals and other organisms

Policy information about [studies involving animals](#); [ARRIVE guidelines](#) recommended for reporting animal research

Laboratory animals	C57Bl/6J mice were purchased from Jackson Laboratory. All animals were male. Upon receipt, animals were housed in a climate-controlled environment with 12 hour light/dark cycles and continued on a high fat diet (HFD, 60% Kcal fat; RD12492; Research Diets, NJ). Animals that were weight-matched into sleeve gastrectomy or sham groups were purchased at 11 weeks of age, allowed to acclimate for 1 week, and operated on at 12 weeks of age. Mice used in the enteral CA7S administration, acute gavage and chronic gavage experiments, as well as the lentiviral knockdown experiments were purchased at 13 to 16 weeks of age and acclimated for at least 1 week before the experiment was performed. All animals were kept on a high-fat diet and glucose tolerance tests were performed when the serum glucose readings were at least 160mg/dL
Wild animals	This study did not involve wild animals
Field-collected samples	This study did not involve samples collected from the field
Ethics oversight	All protocols were improved by the Brigham and Women's Hospital IACUC. Animals were cared for according to guidelines set forth by the American Association for Laboratory Animal Science.

Note that full information on the approval of the study protocol must also be provided in the manuscript.

Human research participants

Policy information about [studies involving human research participants](#)

Population characteristics	Stool samples were prospectively collected from patients pre- and post-sleeve gastrectomy. Patients information was de-
----------------------------	---

Population characteristics

identified prior to sample processing, data collection, and analysis. Subjects were all patients of Dr. Ashley Vernon (co-author) who approached all patients that were slated for bariatric surgery during the enrollment period. Patients had to qualify for bariatric surgery and not have 1) antibiotic use within 3- months of surgery, 2) on immunosuppression, 3) pre-existing immunocompromised state, 4) chronic diarrhea, 5) Ulcerative colitis or Crohn's disease, or 6) prior colon resection. Additionally, patients had to be willing to provide a stool sample pre and post surgery. Patients that are more willing and functionally able to do provide this are represented in the dataset. Again, patients were selected randomly over the course of 1 year with no pre-determined criteria.

Recruitment

Prospective collection. Please see "population characteristics" for patient selection and exclusion criteria. Data from post-sleeve gastrectomy was compared to pre-operative values such that patients served as their own control. the dataset.

Ethics oversight

Brigham and Women's Hospital Institutional Review Boards. All patients were enrolled after informed consent was obtained.

Note that full information on the approval of the study protocol must also be provided in the manuscript.